

**Associate Editor Decision: Publish subject to minor revisions (Editor review)
(10 Mar 2015) by Daniel Obrist**

Comments to the Author:

I am pleased to inform you that I can accept your manuscript based on one final minor revision.

Thank you for this evaluation!

I have received your revised manuscript and your responses to the comments of the reviewers, and I appreciate your thoroughness and clarity in your responses to all reviewer comments. A final criticism from a re-review refers to the clarity of Figure 6 which has not improved and still should be clarified

Thank you for this suggestion, we further improved the clarity of Figure 6.

- please send us a revised figure and let us know how you can improve this figure.

1. We deleted all labels of the single samples
2. We changed the circles to triangles for Yedomia deposit samples
3. We enlarged the circles of the Thermokarst samples
4. All red vector labels are bold right now and the arrow thickness of the red vectors was enlarged as well. We kept the blue vectors and labels in size and style to focus on the red illustrated vectors, which are included in the pc calculation
5. The axis labels were increased as well.

Please find the changes in Figure 6 on page 40 (below). Moreover, I updated my affiliation. No other changes on manuscript were done compared to the previous revised submission.

Best regards,

Jens Strauss

1 Organic matter quality of deep permafrost carbon - a study 2 from Arctic Siberia

3
4 J. Strauss^{1,2*}, L. Schirrmeister¹, K. Mangelsdorf²³, L. Eichhorn⁴³, S. Wetterich¹
5 and U. Herzschuh¹

6 [1]{Alfred Wegener Institute Helmholtz Centre for Polar and Marine Research, Periglacial
7 Research Unit Potsdam, Telegrafenberg A 43, Potsdam, Germany}

8 [\[2\]{Potsdam University, Institute of Earth and Environmental Science, Karl-Liebknecht-Str.
9 24-25, 14476 Potsdam, Germany}](#)

10 [\[23\]{Helmholtz Centre Potsdam GFZ German Research Centre for Geosciences,
11 Telegrafenberg, 14473 Potsdam, Germany}](#)

12 [\[34\]{International Max Planck Research School for Global Biogeochemical Cycles \(Max-
13 Planck-Institute for Biogeochemistry and Friedrich Schiller University\), Burgweg 11, 07749,
14 Jena, Germany}](#)

15 Correspondence to: J. Strauss (Jens.Strauss@awi.de)

17 Abstract

18 The organic carbon (OC) pool accumulated in Arctic permafrost (perennially frozen ground)
19 equals the carbon stored in the modern atmosphere. To give an idea of how Yedoma region
20 permafrost could respond under future climatic warming, we conducted a study to quantify
21 the organic matter quality (here defined as the intrinsic potential to be further transformed,
22 decomposed, and mineralized) of late Pleistocene (Yedoma) and Holocene (thermokarst)
23 deposits on the Buor Khaya Peninsula, northeast Siberia. The objective of this study was to
24 develop a stratigraphic classified organic matter quality characterization. For this purpose the
25 degree of organic matter decomposition was estimated by using a multiproxy approach. We
26 applied sedimentological (grain-size analyses, bulk density, ice content) and geochemical
27 parameters (total OC, stable carbon isotopes ($\delta^{13}\text{C}$), total organic carbon : nitrogen (C/N)
28 ratios) as well as lipid biomarkers (*n*-alkanes, *n*-fatty acids, hopanes, triterpenoids, and
29 biomarker proxies/indices: average chain length, carbon preference index (CPI), and higher

1 plant fatty acid index (HPFA)). Our results show that the Yedoma and thermokarst organic
2 matter qualities for further decomposition exhibit no obvious degradation - depth trend.
3 Relatively, the C/N, and $\delta^{13}\text{C}$, values and the HPFA index show a significantly better
4 preservation of the organic matter stored in thermokarst deposits compared to Yedoma
5 deposits. The CPI data suggest less degradation of the organic matter from both deposits with
6 a higher value for Yedoma organic matter. As the interquartile ranges of the proxies mostly
7 overlap, we interpret this as to indicate comparable quality for further decomposition for both
8 kinds of deposits with likely better thermokarst organic matter quality. Supported by principal
9 component analyses, the sediment parameters and quality proxies of Yedoma and thermokarst
10 deposits could not be separated without ambiguity from each other. This revealed that the
11 organic matter vulnerability is heterogeneous and depends on different decomposition
12 trajectories and the previous decomposition and preservation history. Elucidating this was one
13 of the major novelties of our multiproxy study. With the addition of biomarker data, it was
14 possible to show that permafrost organic matter degradation likely occurs via a combination
15 of (uncompleted) degradation cycles or a cascade of degradation steps rather than as a linear
16 function of age or sediment facies. We conclude that the amount of organic matter in the
17 studied sediments is high for mineral soils and of good quality and therefore susceptible to
18 future decomposition. The missing depth trends reveal that permafrost acts like a giant
19 freezer, preserving the constant quality of ancient organic matter. When undecomposed
20 Yedoma organic matter is mobilized via thermokarst processes, the fate of this carbon
21 depends largely on the environmental conditions; the carbon could be preserved in an
22 undecomposed state till refreezing occurs. If modern input has occurred, thermokarst organic
23 matter could be of a better quality for future microbial decomposition than that found in
24 Yedoma deposits.

25

26 **1 Introduction**

27 During the late Quaternary, the rate of organic matter decomposition in the Arctic has been
28 slower than plant growth, sedimentation, and freezing rates. Thus, a large pool of organic
29 carbon (OC) accumulated in the Arctic and was deeply sequestered in the permafrost.
30 Hugelius et al. (2014) estimates an OC storage of 1300 Gt for the circum-Arctic permafrost
31 region with ~850 Gt OC sequestered in permafrost. This is approximately the carbon stored in
32 the modern atmosphere (Dlugokencky and Tans, 2014). During warming and permafrost

1 thawing, this formerly cryo-sequestered OC gradually entered the modern biogeochemical
2 cycle by microbial turnover. By thawing and microbial activity, the permafrost deposits can
3 turn from a carbon sink to a source (Schuur et al., 2009), releasing greenhouse gases such as
4 carbon dioxide and methane to the atmosphere. Besides the near-surface carbon pool
5 representing the uppermost 3 m below surface, and because of rapid permafrost thaw like
6 thermokarst and thermoerosion, deep OC pools, especially those held in ice-rich permafrost
7 deposits in the Yedoma region, are of great significance for current concerns about the effects
8 of global warming. According to Strauss et al. (2013) and Hugelius et al. (2013), the Yedoma
9 region is defined as the area of potential distribution of late Pleistocene ice-rich and organic-
10 rich silty deposits (Yedoma) covering large areas in Siberia and Alaska. Estimates of OC
11 stored in the Yedoma region amount to 83 ± 12 Gt for late Pleistocene Yedoma deposits (ages
12 shown in Table 1). Due to Holocene warming, subsequent ground ice melt and surface
13 subsidence, thermokarst basins formed and were partly occupied by lakes. Holocene
14 thermokarst deposits (ages shown in Table 1) contain 130 ± 29 Gt organic carbon. In total, the
15 Yedoma region extends to an area of about 1,387,000 km² of which about 70 % is already
16 affected by permafrost degradation (thermokarst) (Strauss et al., 2013). Kuhry et al. (2009)
17 and Schirrmeister et al. (2011a) showed that Yedoma deposits accumulated at fast rates,
18 implying a short time for the organic matter to decay before it became locked into a
19 perennially-frozen state. Therefore, the organic matter availability for microorganisms is
20 expected to be excellent, resulting in great vulnerability to warming ground conditions (Mu et
21 al., 2014). To elucidate how Yedoma region permafrost could respond under conditions of
22 future climatic warming, we studied the organic matter degradation state of Yedoma and its
23 Holocene degradation features (called thermokarst deposits) on Buor Khaya Peninsula,
24 Eastern Laptev Sea. As mentioned above, Strauss et al. (2013) found that thermokarst
25 deposits contain the quantitatively more important carbon pool, but the unsolved question is
26 this: Is the thermokarst organic matter pool as degradable as the frozen late Pleistocene
27 Yedoma, or has the most labile carbon already been emitted due to thermokarst degradation
28 processes? In both kinds of deposits the OC was deeply (deeper than 3 m) incorporated into
29 permafrost (Schirrmeister et al., 2013; Strauss et al., 2013). As shown by models and
30 extrapolation from recent observations, the more southern portions of Yedoma deposits
31 thawed during the last deglaciation, resulting in large emissions of greenhouse gases to the
32 atmosphere (Walter et al., 2007a; Ciais et al., 2012; Walter Anthony et al., 2014). Recent
33 ground warming has been observed in the permafrost zone (Romanovsky et al., 2010), and

1 incubation experiments reveal that permafrost warming is accompanied by a substantial
2 outgassing of greenhouse gases (Lee et al., 2012; Knoblauch et al., 2013; Schädel et al.,
3 2014). As an illustration of the important influence of ground temperature on organic matter
4 degradation, a higher respiration rate at greater depth close to the permafrost table
5 (Mangelsdorf et al., 2009; Waldrop et al., 2010) was found inside the seasonally-thawed
6 active layer and interpreted as a greater lability of the organic matter close to the perennially
7 frozen ground. Focusing on permafrost deposits in the Laptev Sea region, which includes our
8 Buor Khaya study site, Schirrneister et al. (2011a) characterize the Yedoma region
9 permafrost organic matter as weakly decomposed.

10 Biomarkers are used for paleoenvironmental reconstruction of terrestrial permafrost
11 (Andersson et al., 2011) or characterization of permafrost organic matter degradation
12 (Andersson and Meyers, 2012; Vonk et al., 2013; Routh et al., 2014). In our study we
13 estimate molecular markers (*n*-alkanes, *n*-fatty acids, hopanes, and triterpenoids) and use
14 biomarker proxies/indices (absolute lipid concentration, average chain length (ACL), carbon
15 preference index (CPI), hop-17(21)-ene, higher plant fatty acid (HPFA) index, and an
16 Oleanen ratio) to test whether they are useful mirrors of organic matter decomposition, i.e.
17 organic matter state of degradation in permafrost deposits. Rather established methods, both
18 cryolithological (grain-size analyses, bulk density, ice content) and biogeochemical (total
19 organic carbon (TOC_{wt%}), stable carbon isotope ratios ($\delta^{13}\text{C}$ in TOC), total nitrogen (TN), and
20 TOC_{wt%}/TN (C/N) ratios), are applied to our sample set. Finally, principal components
21 analysis (PCA) highlights the relationships between different organic matter degradation
22 proxies.

23 Because the future feedback from the Yedoma region permafrost OC to climate forcing is
24 driven by both (1) the pool size, estimated to be ~211 Gt (Strauss et al., 2013), and (2) the
25 state of degradation of OC stored in the studied deposits, the objective of this study is the
26 development of a stratigraphically differentiated organic matter quality characterization using
27 sample material representative of widespread Yedoma and thermokarst permafrost. We
28 hypothesize increased organic matter degradation during thermokarst processes, but also
29 increased organic matter input during climatically favorable Holocene times.

1 **2 Material and methods**

2 **2.1 Study area**

3 The Buor Khaya Peninsula study site (71°34'N, 132°12'E) is located in the northeastern part
4 of Siberia (Fig. 1). Buor Khaya Peninsula is framed by the Laptev Sea, a shallow
5 epicontinental part of the Arctic Ocean, and geologically by two rift structures (Drachev et al.,
6 1998). Buor Khaya is underlain by continuous permafrost with ground temperatures of less
7 than -11°C (Drozдов et al., 2005). The permafrost thicknesses is estimated to be between 450
8 and 650 m (Romanovskii et al., 2004). Stratigraphically, outcrops from two sediment units are
9 distinguished and studied; (1) ice-rich permafrost, called Yedoma deposits, and (2) deposits in
10 permafrost rapid thaw features, generalized as thermokarst deposits. Three profiles of
11 thermokarst deposits (in a thermokarst basin: Buo-01 and Buo-05; initial thermokarst on top
12 of a Yedoma hill: Buo-03) and two profiles of Yedoma deposits (Buo-02, Buo-04) were
13 studied and sampled. Fig. 1 shows an overview of the sampled profiles and their position
14 relative to each other.

15 **2.2 Field work**

16 Field studies were undertaken in summer 2010 at outcrops situated at the western coast of the
17 Buor Khaya Peninsula. The sediment of the profiles and sub-profiles, exposed at the cliff wall
18 or partly in thermokarst mounds in thaw slumps, were dug by spades and cleaned with hacks.
19 The cryolithology, sediment characteristics, and visible organic matter in the sediments of the
20 chosen sequences were surveyed and described. Moreover, the profiles were photographed
21 and sketched. Sub-profiles were stacked together to create composite profiles. Sampling
22 positions in neighboring sub-profiles were correlated by height estimation using measuring
23 tape. The upper edge of each profile was calibrated with tacheometer measurements (Günther
24 et al., 2012). In the field laboratory all sample volumes were measured with a balance and
25 Archimedes principle, and the absolute ice content was determined by drying the sample. In
26 total, 91 samples were taken and kept cool for transport to laboratories for further analysis.
27 Detailed sampling positions for each profile are shown in Strauss and Schirrmeister (2011).

1 **2.3 Indicators of organic matter quality for further decomposition**

2 To validate and to extend the sedimentological approach used, and to estimate the organic
3 matter quality for further decomposition, lipid biomarkers were measured to estimate the
4 degree of organic matter degradation. For biomarker studies we used a “fingerprint” approach
5 by focusing on identifiable markers related to the state of organic matter degradation. Below,
6 the utilized geochemical indicators and biomarkers are described.

7 **2.3.1 Grain-size analyses**

8 Grain sizes were analyzed using a laser particle sizer (LS 200, Beckmann-Coulter) between
9 0.375 and 1000 μm (Fig. 2, S1). Grain-size calculations were done after Folk and Ward
10 (1957) using Gradistat v8 (Blott and Pye, 2001). A detailed description of these analytical
11 techniques is given in the supplement (supplement section 1.1).

12 **2.3.2 Elemental composition**

13 To determine the total elemental carbon and total nitrogen (TN) content, the samples were
14 measured by a carbon-nitrogen-sulphur analyzer (Vario EL III, Elementar). $\text{TOC}_{\text{wt}\%}$ was
15 measured with a TOC analyzer (Vario Max C, Elementar). The volumetric TOC content
16 ($\text{TOC}_{\text{kg}/\text{m}^3}$) was calculated according to Strauss et al. (2013). A detailed description of this
17 techniques is given in the supplement (supplement section 1.2).

18 The TOC/TN (C/N) ratio has been used as a general indicator of the degree of organic matter
19 decomposition (Stevenson, 1994). Based on the assumption that organic matter components
20 are degraded selectively, degradation modifies elemental compositions and hence C/N in
21 deposits. Because a decrease in the C/N ratio has been observed in aerated deposits with
22 microbial immobilization of TN (nitrogen stays in the system) accompanied by the re-
23 mineralization of TOC (Sollins et al., 1984) and CO_2 emission, this ratio is used in the
24 following way: The higher the C/N ratio, the lower the degree of decomposition.

25 **2.3.3 Bulk density and volumetric carbon content**

26 BD was calculated using equation 1.

$$27 \text{BD} [10^3 \text{kg}/\text{m}^3] = \frac{\text{sample dry weight} [10^3 \text{kg}]}{\text{sample volume} [\text{m}^3]} \quad (1)$$

1 Estimating the BD is required to convert the measured-weight-based $\text{TOC}_{\text{wt}\%}$ content per
2 sample to a volume-based value. Thus, the $\text{TOC}_{\text{kg}/\text{m}^3}$ was calculated according to equation 2:

$$3 \quad \text{TOC}_{\text{kg}/\text{m}^3} = \text{BD} [10^3 \text{kg}/\text{m}^3] \times \frac{\text{TOC}_{\text{wt}\%}}{100} \quad (2)$$

4 **2.3.4 Carbon isotope studies**

5 Stable TOC carbon isotopes were determined with a Finnigan MAT Delta-S mass
6 spectrometer combined with a FLASH elemental analyzer and a CONFLO III gas mixing
7 system. A detailed method is given in the supplement (supplement section 1.4). The stable
8 carbon isotopes of OC reflect (1) initial contribution from different plant species and plant
9 components, and (2) subsequent degradation processes (Gundelwein et al., 2007). Assuming
10 constant photosynthetic isotope fractionation in source plants in the region (C_3 plants are
11 ubiquitous in the Arctic, Tieszen (1973)), we use $\delta^{13}\text{C}$ ratios as a degradation proxy. After
12 Heyer et al. (1976), decomposition discriminates against the lighter isotope (^{12}C), resulting in
13 more negative $\delta^{13}\text{C}$ ratios. Thus, this proxy is used in the following way: Lower (more
14 negative) $\delta^{13}\text{C}$ values are connected to less degraded material, while higher (less negative)
15 $\delta^{13}\text{C}$ values reflect greater decomposition.

16 Ages were determined by radiocarbon dating of selected macroscopic plant remains
17 performed at the Poznań Radiocarbon Laboratory, Poland (Goslar et al., 2004). The presented
18 radiocarbon ages are uncalibrated ages; Table 1 includes calibrated ages as well. Radiocarbon
19 ages are given in year before present (a BP).

20 **2.3.5 Lipid biomarkers**

21 To look more closely at the molecular composition, we used specific lipid biomarkers.
22 Molecular fossils or biomarkers were studied by chromatography methods coupled with mass
23 spectrometers. Characteristic fractions like *n*-alkanes, *n*-fatty acids, sterols, and hopanes were
24 isolated. Because the $\text{TOC}_{\text{wt}\%}$ in the profiles is not equally distributed, we calculated and
25 visualized the biomarker concentration as $\mu\text{g}/\text{gTOC}_{\text{wt}\%}$ and $\mu\text{g}/\text{gSediment}$ ($\mu\text{g}/\text{gSed}$). For the
26 results, we focus on $\mu\text{g}/\text{gTOC}_{\text{wt}\%}$. Every radiocarbon-dated sample and additional samples
27 were used for biomarker analysis. In total 25 biomarker samples were analyzed. Independent
28 from $\text{TOC}_{\text{wt}\%}$, the sample selection for biomarkers was based on stratigraphic position with
29 the aim to cover the maximum time period.

30 **Extraction and fraction separation**

1 For lipid biomarker analyses 2-12 g of ground sediment was weighed in an extraction cell
2 with an accelerated solvent extractor (ASE 200, Dionex). Samples were extracted with
3 dichloromethane/methanol (99:1). Each sample was held in a static phase for 20 minutes at 75
4 °C (after 5 minutes heating, no preheating) at a pressure of 5 MPa. Afterwards, the dissolved
5 compounds were concentrated with a Turbo Vap (Zymark) closed cell concentrator and
6 further dried by evaporating the solvent in a stream of nitrogen gas. After that, internal
7 standards (5 α -androstane for the aliphatic fraction, ethylpyrene for the aromatic fraction, 5 α -
8 androstan-17-on for nitrogen-, sulfur-, and oxygen- (NSO-) containing compounds, and erucic
9 acid for the NSO fatty acid fraction) were added. The amount of internal standards depended
10 on the TOC_{wt%} content (<10wt%: 8 μ g; >10 to \leq 25wt%: 20 μ g; >25wt%: 50 μ g). After the
11 removal of the *n*-hexane-insoluble fraction (by the addition of a large excess of *n*-hexane,
12 called 'asphaltene' precipitation), the hexane-soluble portion of the extract was separated by
13 medium-pressure liquid chromatography (MPLC; (Radke et al., 1980) into fractions of
14 different polarity (aliphatic and aromatic hydrocarbons as well as polar hetero (NSO)
15 components). Afterwards, the NSO fraction was split into a fatty acids and an alcohol fraction
16 using a KOH-impregnated silica gel column (Schulte et al., 2000).

17 For this study, the focus was placed on the aliphatic fraction (containing *n*-alkanes and
18 triterpenoid compounds) and the NSO fraction (containing *n*-fatty acids). The fractions were
19 measured by gas chromatography–mass spectrometry (GC–MS). All compounds of interest
20 were identified using the Xcalibur software (Thermo Fisher Scientific).

21 **GC-MS measurement and compound quantification**

22 The *n*-alkanes, *n*-alcohols, hopenes (hop-17(21)-ene), and other triterpenoids (β -amyrin
23 (olean-12-en-3 β -ol), Olean-12-ene, and Olean-13(18)-ene) were measured with a GC-MS
24 system (GC: Trace GC Ultra; MS: DSQ, both Thermo Fisher Scientific). Prior to the
25 measurements, the *n*-fatty acids were methylated with diazomethane and the alcohols were
26 silylated with *N*-methyl-*N*-trimethylsilyltrifluoroacetamide (MSTFA). The GC was equipped
27 with a programmable temperature vaporization (PTV) injector system (starting temperature of
28 50 °C; heating rate of 10°C/sec to 300°C; isothermal holding time of 10 minutes; operated in
29 splitless mode) and a fused silica capillary column (SGE BPX5, 50 m length, 0.22 mm inner
30 diameter, 0.25 μ m film thickness). For the measurements the GC oven was programmed with
31 a starting temperature of 50°C, a heating rate of 3°C/min to 310°C, and an isothermal holding
32 time of 30 minutes. Helium with a constant flow rate of 1 ml/min was used as a carrier gas.

1 For the *n*-fatty acid fraction a different temperature program (starting temperature of 50°C, 1
2 min isotherm, heating rate of 3°C/min to 350°C, isothermal holding time 25 minutes) was
3 used. For compound identification, the gas chromatograph was linked to a mass spectrometer,
4 which was operated in electron impact ionization mode at 70 eV. The temperature of the ion
5 source was set to 230°C. Full scan mass spectra were recorded from *m/z* 50 to 600 Da at a
6 scan rate of 2.5 scans/sec. For the *n*-fatty acids fraction the scan rate was *m/z* 50 to 650 Da.

7 Quantification of *n*-alkanes, *n*-fatty acids, and β-amyrin was done in the GC-MS total ion
8 current chromatogram by relating the peak area of the target compound to the peak area of an
9 internal standard of known concentration. Other triterpenoids like Olean-12-ene, Olean-
10 13(18)-ene, and hopene were quantified using the *m/z* 191 mass trace relative to the peak area
11 of the β,β-diploptene (in the *m/z* 191 mass trace), the concentration of which was calculated
12 in the total ion current chromatogram relative to the internal standard (5α-androstane).

13 **2.3.6 Biomarker proxies/indices**

14 **Absolute lipid concentration**

15 The absolute lipid concentration is used as rough estimator of organic matter quality for
16 degradation in the following sense: The higher the concentration, the better the conservation
17 of the lipid, and the better the quality of the organic matter.

18 **Carbon preference index**

19 The CPI was introduced by Bray and Evans (1961) as the ratio of odd- to neighboring even-
20 numbered alkanes, which is a measure of the alteration of organic matter. Here we use the
21 improved formula after Marzi et al. (1993). In addition, we also applied the CPI for fatty acids
22 in which even-numbered fatty acids predominate over adjacent odd *n*-fatty acids (Glombitza
23 et al., 2009).

$$24 \text{ CPI} = \frac{(\sum_{i=n}^m C_{2i+1}) + (\sum_{i=n+1}^{m+1} C_{2i+1})}{2 \times (\sum_{i=n+1}^{m+1} C_{2i})} \quad (3)$$

25 *n*: starting dominating chain length/2; *m*: ending dominating chain length/2; *i*:
26 index (carbon number); *C*: concentration

27 The CPI is used as a degradation/alteration proxy by quantifying the odd/even (*n*-alkanes, Fig.
28 S2) or even/odd (*n*-fatty acids, Fig. S3) of the carbon chains (Bray and Evans, 1961;

1 Glombitza et al., 2009). A low CPI means mature/degraded organic matter (e.g. CPI of crude
2 oil ~1).

3 **Average chain length**

4 As introduced by Poynter (1989), the *n*-alkane ACL value is the concentration-weighted mean
5 of different carbon chain lengths in a geological sample. For *n*-alkanes we use the C₂₃-C₃₃
6 interval, for *n*-fatty acids the C₂₀-C₃₄:

$$7 \text{ ACL} = \frac{\sum i \times C_i}{\sum C_i} \quad (4)$$

8 *i*: index (carbon number); *C*: concentration

9 The ACL is a rough OC source parameter. A schematic showing different chain lengths in
10 different organisms is given in Fig. S4. The higher C₃ land plants are expected to have an
11 ACL of ~28-29.

12 **Hop-17(21)-ene**

13 We use hop-17(21)-ene as another marker for low-maturity organic material. The hop-17(21)-
14 ene is produced by bacteria. The assumption here is that during degradation and diagenesis
15 the hop-17(21)-ene will be transformed into saturated hopane (Luo et al., 2012).

16 **Higher Plant Fatty Acid index**

17 The ratio of the major even wax alcohols over the sum of major odd wax alkanes plus even
18 alcohols was introduced by Poynter (1989) as the Higher Plant Alcohol (HPA) index. It is
19 applied as an indicator for chemical degradation of the wax components. Based on this index,
20 but using fatty acids instead of alcohols, we developed the HPFA index. The general
21 assumption for this index is that it reflects the preservation degree of the organic matter due to
22 the higher lability of *n*-fatty acids in relation to *n*-alkanes.

$$23 \text{ HPFA} = \frac{\sum \text{n-fatty acids}_{C_{24}, C_{26}, C_{28}}}{\sum \text{n-fatty acids}_{C_{24}, C_{26}, C_{28}} + \sum \text{n-alkanes}_{C_{27}, C_{29}, C_{31}}} \quad (5)$$

24 The HPFA ratio cannot be considered an absolute index of degradation, but is an indicator of
25 the relative amounts of the more labile fatty acids that remain in a sample. Since *n*-alkanes are
26 preserved preferentially compared to *n*-fatty acids, a decrease in this index indicates increased
27 decomposition (the more degraded, the lower the HPFA index).

28 **Oleanen ratio**

1 β -amyrin (olean-12-en-3 β -ol) is a triterpenoid produced by higher land plants. As a first
2 degradation step, β -amyrin is expected to lose its hydroxy-group and will be transformed to
3 Olean-12-ene. A second step would be a shift of the double bond forming Olean-13(18)-ene.
4 Thus, fresh organic material is associated with a lower oleanen ratio, while more degraded
5 organic matter is reflected in a higher ratio. This index is calculated:

$$6 \text{ oleanen ratio } [\%] = \frac{\text{Olean-12-ene} + \text{Olean-13(18)-ene}}{\beta\text{-amyrin}} \times 100 \quad (6)$$

7 **Acetate**

8 Pore water was obtained from each sample by centrifugation in specific pore water tubes.
9 Water extracts were analyzed twice using ion chromatography with conductivity detection
10 (ICS 3000, Dionex). An analytical column (AS 11 HC, 2 \times 250 mm, Dionex) was used at
11 constant 35°C. The sample was eluted with KOH solution of varying concentration over time.
12 The initial concentration was 1.4 mM. Between 0 and 6 minutes, the KOH solution was
13 increased at a constant rate to 1.6 mM. Between 6 and 12 minutes the solution was increased
14 to 10.0 mM KOH and a concentration of 15.0 mM KOH was reached at 22 minutes. After 32
15 minutes, 60.0 mM KOH concentration was achieved, and maintained for 1 minute, followed
16 by a rapid decrease to 1.4 mM after 33 minutes where samples were fixed for 45 minutes to
17 equilibrate the system. For quantification of acetate, standards containing the investigated
18 compound were measured. The standard deviation of the sample and of standard
19 quantification was <5%. Because acetate can act as excellent feedstock for microbes (Smith
20 and Mah, 1980; Vieth et al., 2008) and it has been shown that acetate was rapidly consumed
21 in the presence of oxygen and nitrate (Kuesel and Drake, 1995), we use the acetate pore water
22 concentrations in the different deposits as a parameter to assess the quality of the organic
23 matter and to compare the potential of the different deposits for future microbial degradation.

24 **2.4 Statistical methods**

25 **2.4.1 Significance testing**

26 For testing the samples concerning their statistical distribution, the Shapiro-Wilk normality
27 test was applied. Because of non-normal distribution, we used the Mann-Whitney-Wilcoxon
28 test for significance testing of Yedoma and thermokarst samples. For comparing the different
29 five profiles, we used Kruskal-Wallis rank sum test.

1 **2.4.2 Principal component analysis**

2 Multivariate statistical techniques, like the PCA used here, allow the analysis of multiple
3 variables in order to investigate connections between the different degradation proxies. Prior
4 to the PCA, concentration data were transformed using a $\log(x+1)$ transformation. As the
5 square root transformation is commonly applied to count data, especially if the values are
6 mostly rather small, we decided to use this weaker (compared to logarithm) transformation for
7 the TOC ($_{\text{wt}\%}$ and $_{\text{kg/m}^3}$) data. Both transformations were applied to reduce right skewness and
8 to put the parameters on the same scale. We performed three PCA runs. First, a PCA of the
9 sediment parameters was implemented to infer differences between Yedoma and thermokarst
10 deposits. Second, a PCA of biomarker proxies was performed. For this purpose, other
11 characteristics were added as supplementary variables (TOC $_{\text{wt}\%}$, TOC $_{\text{kg/m}^3}$, C/N, $\delta^{13}\text{C}$, grain
12 size, BD, ice content, and depth) without inclusion in the PCA calculation. These
13 supplementary variables have no influence on the PCA and were plotted afterwards in the
14 PCA biplot. Third, a PCA was conducted on samples of the major odd *n*-alkanes to infer
15 possible changes of the source organisms with the same supplementary variables as described
16 above to relate the different biomarker proxies to each other. Computations were performed
17 using the “vegan” package of R software (Oksanen, 2013).

18 **3 Results**

19 Stratigraphically, there are two types of deposition units at the study site. The first unit is
20 composed of Yedoma deposits. The second unit represents thermokarst deposits resulting
21 from thermal degradation of Yedoma. Grain-size distributions (Fig. 2, S1) and PCA of
22 sediments illustrate that thermokarst deposits are made up of degraded Yedoma sediments.
23 After Gubin and Veremeeva (2010) and Zanina et al. (2011) the Yedoma deposits soil types
24 are mainly less-developed cryopedoliths containing more-developed paleocryosol parts (Fig.
25 3 and 4, labeled and grey-shaded areas).

26 **3.1 Organic matter quality of Yedoma deposits**

27 **3.1.1 Sedimentological and biogeochemical proxies**

28 The radiocarbon ages (Table 1, Fig. S5) of the Yedoma deposits range from infinite ages
29 ($>55,000$ a BP) at the very bottom to 30,100 a BP at the uppermost sampled Yedoma unit.
30 This is comparable to other Yedoma sequences in the region (Schirrmeister et al., 2011b). The

1 mean grain sizes show a decreasing trend in the Buo-04 lower Yedoma profile, from 28 μm at
2 the bottom to 11 μm in the upper part of Buo-04-A. The Buo-02 Yedoma profile shows no
3 trend, but exhibits a more heterogeneous mean-grain size including three maxima at 22.5 m
4 above sea level (a.s.l.) (32 μm), 23.7 m a.s.l. (34 μm), and 25.5 m a.s.l. (33 μm).
5 Nevertheless, all Yedoma deposit samples are classified as poorly-sorted medium-to-coarse
6 silts with a stable low clay fraction (<15%).

7 The $\text{TOC}_{\text{wt}\%}$ contents vary from 0.2 wt% at 5 m a.s.l to 24.0 wt% in a peaty paleocryosol
8 horizon at 24 m a.s.l. (Fig. 3). The mean $\text{TOC}_{\text{wt}\%}$ content is 2.4 wt% (median 0.97 wt%).
9 Calculating the $\text{TOC}_{\text{kg}/\text{m}^3}$ according to Strauss et al. (2013) by utilizing the BD (between 0.1
10 and 1.5 $10^3\text{kg}/\text{m}^3$ ($10^3\text{kg}/\text{m}^3 = \text{g}/\text{cm}^3$)) and ice content (without ice wedges; 21 to 90 vol%), the
11 Yedoma sediments contain from 3 to 46 $\text{kg C}/\text{m}^3$ with a mean of 14 $\text{kg C}/\text{m}^3$ (median 9 kg
12 C/m^3). The maxima correspond to the peaty horizons with large $\text{TOC}_{\text{wt}\%}$ contents and a low
13 BD. Within the paleocryosol horizons, located at 6.8, 24.0 to 24.5, 24.8, and 27.8 to 28.9 m
14 a.s.l., maxima in the C/N ratio are observable. The C/N range in these horizons is 8 to 31. In
15 the cryopedolith profile parts the C/N maximum is reached at the lowermost Buo-04-C sub-
16 profile (17.7 and 16.7). The C/N of the rest of the Yedoma profile falls between 4.1 (at Buo-
17 02-C, 23.7 m a.s.l.) and 14.3 (below the paleocryosol at 23.5 m a.s.l.)

18 The $\delta^{13}\text{C}$ of the Yedoma deposits ranges between -29.0 and -24.7 ‰. The minima fit well to
19 the maxima of the C/N ratio in the paleocryosol horizons at 6.8, 24.0 to 24.5, 24.8, and 27.8 to
20 28.9 m a.s.l. The minimum C/N of the Buo-02-C sub-profile corresponds approximately to
21 the $\delta^{13}\text{C}$ maximum (-25.0 to -24.7 ‰).

22 **3.1.2 Biomarker proxies/indices**

23 A series of long-chain *n*-alkanes that exhibit a strong odd-carbon preference ranging from *n*-
24 C_{21} to *n*- C_{33} are recognized in all Yedoma samples (Fig. S2). Moreover, the *n*-alkanes show a
25 unimodal distribution maximizing at the C_{27} , C_{29} , or C_{31} *n*-alkane (Fig. S2). The *n*-fatty acids
26 show strong even-over-odd carbon number predominance and a bimodal distribution ranging
27 from C_{14} to C_{30} (Fig. S3). The maxima are generally located at *n*- C_{16} in the lower carbon
28 number range and at *n*- C_{24} in the higher carbon number range. Total *n*-alkanes and *n*-fatty
29 acids concentrations related to $\text{TOC}_{\text{wt}\%}$ and sediment weight show a homogeneous pattern
30 similar to that of the $\text{TOC}_{\text{wt}\%}$ and C/N values. The *n*-alkane concentration ranges from 3 to 75
31 $\mu\text{g}/\text{gSed}$ (mean 20 $\mu\text{g}/\text{gSed}$) and from 387 to 1715 $\mu\text{g}/\text{TOC}_{\text{wt}\%}$ (mean 1132 $\mu\text{g}/\text{TOC}_{\text{wt}\%}$). The

1 *n*-fatty acids range from 4 to 306 $\mu\text{g/gSed}$ (mean 51 $\mu\text{g/gSed}$) and from 475 to 4669 $\mu\text{g/TOC}$
2 (mean 2196 $\mu\text{g/TOC}_{\text{wt}\%}$).

3 This Yedoma series shows distinct preference between even and odd carbon. The mean CPI
4 values of the *n*-alkanes (12.2, ranging between 8.3 and 15.9) are higher than the CPI values of
5 the *n*-fatty acids (4.9, ranging between 3.8 and 7.6). Because *n*-fatty acids are functional
6 compounds (including a functional group, e.g. a carboxyl group), their degradation rates are
7 much higher compared to those of *n*-alkanes (Poynter and Eglinton, 1990). This statement is
8 also based on the assumption of similar sources. The ACL of the *n*-alkanes and *n*-fatty acids
9 is very stable at around 28.4 (range 27.6 to 29.2) and 25.0 (range 23.8 to 25.6), respectively.

10 Relatively higher hop-17(21)-ene concentrations are used as an indicator for lower organic
11 matter degradation state. In the lower Yedoma profile the hop-17(21)-ene ranges from 0.0
12 $\mu\text{g/gTOC}$ at the lowermost and uppermost samples (4.3 and 18.5 m a.s.l.) to the overall
13 maximum at the Buor Khaya site (19.4 $\mu\text{g/gTOC}$) at 9.1 m a.s.l. At Buo-02, the hop-17(21)-
14 ene concentration is lower compared to the other Yedoma profile with a mean of 1.9
15 $\mu\text{g/gTOC}_{\text{wt}\%}$ and a maximum of 7.7 $\mu\text{g/gTOC}_{\text{wt}\%}$ in the potentially Holocene-contaminated
16 uppermost sample. The HPFA ratio for the Yedoma samples is very stable around the mean
17 value of 0.50 (median 0.54) with a minimum at 18.5 m a.s.l. (0.15) and a maximum at the
18 uppermost sample (0.69) at 29.7 m a.s.l. For Yedoma, the Oleanen ratio is 0.0 (except a ratio
19 of 10.0 at the uppermost sample). The acetate content of the Yedoma sample is between 0.6
20 and 57.5 mg/L with a mean of 6.7 mg/L (median 1.2 mg/L).

21 **3.2 Organic matter quality of thermokarst deposits**

22 **3.2.1 Sedimentological and biogeochemical proxies**

23 The radiocarbon dating shows Holocene ages between 8140 ± 50 and 3665 ± 35 a BP (Fig. S6,
24 Table 1). The lowermost Buo-05-C profile shows an age inversion for the two samples, (0.3
25 and 2.2 m a.s.l.). The mean grain size at Buo-05 from the bottom to 6.7 m a.s.l. is 13 μm .
26 Above, the mean grain size increases to 19 μm . The Buo-05 clay fraction is stable at a low
27 level (<15%). The Buo-01 profile shows a very scattered grain size ranging from 4 to 44 μm
28 mean grain size. For the whole dataset, there is a maximum in the clay fraction (35%) in the
29 peat horizon at 8.7 m a.s.l. Buo-03 shows a slight decrease from 18 to 11 μm . All thermokarst
30 deposits are classified as (very) poorly-sorted silts. Similar to the Yedoma deposits, the BD of

1 the thermokarst deposits is between 0.1 and 1.5 10³kg/m³ and the ice content (without the ice
2 wedges) is 23 to 87 wt% (Fig. 4).

3 The mean TOC_{wt%} contents of the thermokarst deposits, 4.7 wt% (median 1.7 wt%), are
4 higher compared to Yedoma deposits, varying between 0.2 wt% and 43.0 wt%. Minimum and
5 maximum TOC_{wt%} both occur at Buo-01 and exhibit the same scatter as in the grain sizes.
6 TOC_{kg/m³} ranges between 2.8 and 93.5 kg C/m³ (mean 24 kg C/m³, median 19 kg C/m³).

7 At Buo-05 the C/N ratio is stable around 9 to 10 (Fig. 4), except for a paleocryosol horizon at
8 9.2 m a.s.l. that shows a value of 22. At Buo-01, the C/N ratio below the paleocryosol horizon
9 is remarkably low, between 2 and 9, followed by the overall maximum in the peaty horizon
10 with a ratio of 34. The Buo-03 cryopedolith samples show C/N ratios around 10, while the
11 paleocryosol samples exhibit C/N ratios from 16 to 19. The δ¹³C values range between -29.5
12 and -25.0 ‰, with minima corresponding to the C/N maxima at the paleocryosol horizons
13 (anti-correlated to the C/N, Fig. 5a).

14 **3.2.2 Biomarker proxies/indices**

15 The absolute lipid concentration of *n*-alkanes are in the same range but slightly higher
16 compared to the Yedoma profiles. The *n*-alkane average is 1275.7 μg/gTOC_{wt%} (median
17 1260.1 μg/gTOC_{wt%}), ranging from 599.7 (8.7 m a.s.l.) to 1907.2 μg/gTOC_{wt%} (29.5 m a.s.l.).
18 The *n*-fatty acids average is nearly double that found in the Yedoma samples. On average,
19 4096.1 μg/gTOC_{wt%} (median 3805.7 μg/gTOC_{wt%}) are stored in the thermokarst deposits of
20 Buor Khaya, ranging from 554.5 (uppermost Buo-01 sample) to 11013.3 (uppermost Buo-03
21 sample) μg/gTOC_{wt%}.

22 A series of long-chain *n*-alkanes were recognized in all thermokarst samples with a strong odd
23 carbon number preference ranging from *n*-C₂₁ to *n*-C₃₃. Nearly all samples show a unimodal
24 distribution of *n*-alkanes maximized at C₂₇, C₂₉, or C₃₁ (Fig. S2). Sample Buo-03-A-03 alone
25 does not fit into this scheme because it maximizes at *n*-C₂₅. Compared to Yedoma samples,
26 the short-chain fraction < *n*-C₂₇ is more pronounced (Fig. S2). The *n*-fatty acids show strong
27 even-carbon-number preference and a bimodal distribution between *n*-C₁₄ and *n*-C₃₀ (Fig. S3),
28 but the *n*-C₁₆ is less pronounced than in the Yedoma deposits. An exception to this is found in
29 sample Buo-01-A-02, where the C₁₆ monomer reaches the overall maximum of the
30 distribution. Apart from that, the maxima are generally located at the C₂₄ *n*-fatty acid.

1 The *n*-alkane CPI of thermokarst averages 9.6 (median 9.3) and is lower compared to the
2 Yedoma deposits, although the CPI values are in the same range (between 7.0 and 15.3). The
3 CPI of the fatty acids ranges from 4.0 to 9.0 (mean 5.3, median 4.9). The ACL of *n*-alkanes
4 and fatty acids reveal a homogeneous signal between 27.2 and 29.2 (mean 28.3) for *n*-alkanes
5 and 23.6 to 25.6 (mean 24.8) for *n*-fatty acids.

6 Except for the maximum value of 16.1 $\mu\text{g/gTOC}_{\text{wt}\%}$ at 8.7 m a.s.l., the hop-17(21)-ene
7 concentration at Buo-05 varies between 0.1 and 4.9 $\mu\text{g/gTOC}_{\text{wt}\%}$. Buo-01 paleocryosol values
8 are 0.9 (8.7 m a.s.l.) and 8.4 at the lowermost sample (7.8 m a.s.l.). For Buo-03 the hop-
9 17(21)-ene concentration ranges from 5 $\mu\text{g/gTOC}_{\text{wt}\%}$ up to 8 $\mu\text{g/gTOC}_{\text{wt}\%}$.

10 The HPFA ratio for the Buo-05 thermokarst samples is high, between 0.6 and 0.8; only the
11 uppermost sample (9.3 m a.s.l.) shows a lower value of 0.2. The Buo-01 profile decreases
12 from 0.7 at the lowest sample to 0.2 at the top. Buo-03 shows high parameter values of 0.8
13 and 0.9. The Oleanen ratio for the thermokarst deposits ranges between 0 (Buo-01) and 13.8
14 (Buo-03). The overall mean Oleanen ratio in thermokarst is 3.7 (median 2.2), which is
15 remarkably higher compared to the Yedoma deposits.

16 The acetate content of the thermokarst samples is between 0.4 and 109.4 mg/L with a mean of
17 23.5 mg/L (median 2.8 mg/L). Large acetate contents are found especially in the middle part
18 of Buo-05, from 3.4 m a.s.l. (74.1 mg/L) to 6.1 m a.s.l. (109.4 mg/L), and in the uppermost
19 Buo-03 sample (35.3 mg/L).

20 **3.3 Statistical methods**

21 **3.3.1 Significance testing**

22 Except for the Yedoma CPI, the Yedoma HPFA and the thermokarst hop-17(21)-ene Shapiro-
23 Wilk normality test reveals a non-normal distribution. Based on this, we chose non-parametric
24 significance testing. This reveals significant differences for TOC, C/N, $\delta^{13}\text{C}$ and HPFA on the
25 stratigraphical level (Yedoma vs. thermokarst, Mann-Whitney-Wilcoxon test, Tab. S1). On
26 the profile level, we found significant differences for C/N, $\delta^{13}\text{C}$ and HPFA by applying the
27 Kruskal-Wallis test (Tab. S1).

1 **3.3.2 Principal component analyses**

2 The first PCA diagram (Fig. 6a) shows that thermokarst sediments, especially at Buo-05,
3 could not be separated from Yedoma deposits. This diagram, including the first two principal
4 components, explains 79 % (pc1 57%, pc2 22%) of the total data set variance. The second
5 PCA diagram (Fig. 6b) illustrates that biomarker quality estimators in Yedoma samples have
6 slightly lower variability because they cluster in an area at pc1 and pc2>0, while the
7 thermokarst samples do not cluster. In this diagram 53 % of the data set variance is explained.
8 Moreover, this PCA shows that there is good consistency between the CPI_{alkane} quality
9 estimator and the C/N ratio (Fig. 6b). The PCA of the *n*-alkane chain length (Fig. 6c) shows
10 that the best separating variables for thermokarst are the shorter-chain *n*-alkanes (C₁₇, C₁₉, and
11 C₂₁), contrary to C₂₉ for the majority of the Yedoma samples. The pc1 explains 39% and pc2
12 explains 29% (total 68%) of the data set variance.

13

14 **4 Discussion**

15 The Buor Khaya Peninsula is a typical Yedoma hill - thermokarst basin landscape of the
16 Yedoma region (Strauss et al., 2013). The Yedoma deposits cover ~15% of the peninsula
17 (Günther et al., 2013), which is less than the Yedoma region mean of 30%, but inside the
18 overall range of Yedoma deposit coverage (Grosse et al., 2013; Strauss et al., 2013). Thus, the
19 current study of Yedoma and thermokarst deposits is representative for an area covered by
20 similar permafrost deposits of late Pleistocene and Holocene age.

21 **4.1 Sediment facies**

22 The grain-size distribution curves (Fig. 2, S1) indicate a constant deposition environment for
23 the Yedoma sequences. According to Strauss et al. (2012), there have been stable deposition
24 conditions during Yedoma accumulation; this hypothesis is supported by the data presented
25 here. The three thermokarst profiles include three different kinds of thermokarst deposits.
26 Buo-05 is dominated by a lake facies containing valves of two freshwater ostracod taxa:
27 *Cytherissa lacustris* and *Cypria* sp. Moreover, shells have been found in Buo-05 (Strauss and
28 Schirrmeister, 2011). An ice wedge is located next to Buo-01, which points to sub-aerial
29 conditions like a polygon mire. Buo-03 is interpreted as initial thermokarst on top of a
30 Yedoma hill. Thus, the grain-size distributions of Buo-05 and Buo-01 reveal that the
31 thermokarst is granulometrically composed of the same material as Yedoma. The grain-size

1 distributions in Buo-03 paint a different picture. This distribution is likely caused by the early
2 state of thermokarst development dominated by peat aggradation. This peat can act like a
3 selective sediment trap influencing the grain-size distributions, e.g. by producing a less
4 distinct coarse silt-fine sand peak.

5 **4.2 Organic matter degradation**

6 The organic matter proxies of Yedoma deposits are less variable than those of thermokarst
7 deposits (Buo-01 and 03). Except for the paleocryosols, the cryopedolith parts of the Yedoma
8 and the Buo-05 thermokarst profile reveal a rather homogenous picture (Fig. 3, 4, S5, S6).
9 Constant grain-size distributions, less $\text{TOC}_{\text{wt}\%}$, and smaller absolute lipid concentration
10 scattering reveal that the OC stored in the Yedoma deposits has likely been kept perennially
11 frozen since incorporation. The organic matter signatures (Fig. 4, S2, and S3) as well as the
12 grain-size distributions (Fig. 2, S1) of thermokarst deposits, especially in Buo-01 and Buo-03,
13 show broader variations. This is caused by a more complex degradation and re-deposition
14 history due to reworking. The degradation markers of organic matter found in the
15 paleocryosol parts of all profiles reveal a less-degraded state, indicating that the organic
16 matter in these portions is the best preserved.

17 The mean $\text{TOC}_{\text{wt}\%}$ content for Yedoma deposits is comparable to other sites (Fig. S7) in the
18 Yedoma region (Schirrmeister et al., 2011b; Schirrmeister et al., 2013). Intense accumulation
19 and frozen preservation of plant remains (14 kgC/m^3 for Yedoma and 24 kgC/m^3 for
20 thermokarst deposits) is caused by syngenetic permafrost formation in polygonal tundra
21 landscapes over long periods in the Quaternary (Schirrmeister et al., 2013). But comparing the
22 studied deposits to the overall Yedoma region mean (19 kgC/m^3 for Yedoma deposits and 33
23 kgC/m^3 (disregarding wedge-ice content) for thermokarst deposits, Strauss et al. (2013)) on
24 Buor Khaya Peninsula reveals that both deposit types contain less OC. Nevertheless, these
25 numbers show that such deposits comprise a large pool of dormant carbon, which could be
26 reactivated due to permafrost thawing. Moreover, thermokarst deposits seem to be the
27 quantitatively more important OC pool (Yedoma : thermokarst carbon ratio ~2:3). The higher
28 carbon inventory in thermokarst deposits is partially related to a concentration effect for
29 reworked Yedoma OC due to thaw subsidence progression including ground ice loss plus
30 input of Holocene OC. Together with ecosystem recovery, thermokarst basins can act as a
31 local sink for portions of the carbon released from thawing permafrost deposits (van
32 Huissteden and Dolman, 2012). Nevertheless, at the same time thermokarst lakes also

1 promote intense organic matter degradation including methane production in the anaerobic
2 environments of organic-rich lake sediments and unfrozen deposits (Walter et al., 2007b;
3 Shirokova et al., 2013). To answer this question arisen in the introduction, if the thermokarst
4 organic matter pool is as degradable as the frozen late Pleistocene Yedoma we visualized the
5 stratigraphically differentiated main proxies in Fig. 7.

6 In our study the C/N data shows an overlap (Fig. 7b). The average values are relatively close
7 together for all profiles, but the differences are statistically significant (Tab. S1). Thus, the
8 C/N medians and means hint at a lower degradation state/better organic matter quality of
9 thermokarst deposits (especially Buo-03 and Buo-03). Moreover, in both Yedoma and
10 thermokarst deposits the same pattern is visible: A positive linear relationship exists between
11 $\text{TOC}_{\text{wt}\%}$ and C/N ratios (Fig. 5b). In soil science literature it is agreed that the elemental
12 composition of organic matter is affected by the degree of humification and microbial
13 activities that metabolize the organic matter (Kumada, 1987). Ongoing organic-matter
14 decomposition will release stored C to the atmosphere and N to the soil (Weintraub and
15 Schimel, 2005), resulting in a lower C/N ratio for more-degraded deposits (Gundelwein et al.,
16 2007). This was found in (sub-) arctic peat deposits and soils, where the C/N ratio decreases
17 with depth (Kuhry and Vitt, 1996; McKane et al., 1997; Ping et al., 1998). Because a high TN
18 content can promote stabilization of organic matter at late stages of decomposition (Berg,
19 2000), this further supports the interpretation that a low C/N ratio indicates
20 recalcitrant/matured organic matter (Rumpel and Kögel-Knabner, 2011). Schädel et al. (2014)
21 found, with incubation studies, that the C/N ratio is a good estimator for organic-matter
22 decomposability/vulnerability. Although the C/N ratios are lower than in arctic peat deposits
23 (Hugelius et al., 2012; Routh et al., 2014), the ratios are still in the range of or higher than
24 those found in many other deep mineral soils of the temperate zone (Jenkinson et al., 2008;
25 Rumpel and Kögel-Knabner, 2011). Thus, both Yedoma and thermokarst deposits show
26 relatively good organic matter quality for microbial decay after becoming available by thaw.
27 The C/N ratios, especially for the paleocryosols, suggest that good quality organic matter was
28 preserved (by sub- or near 0°C temperatures during thermokarst processes) for future
29 decomposition. This is shown by the $\delta^{13}\text{C}$ ratio as well. Neglecting the influence of different
30 sources of organic matter on the $\delta^{13}\text{C}$ ratio, which is justified by constant ACL values of >28
31 (higher land plants, Fig. S4) for Yedoma and thermokarst deposits, the $\delta^{13}\text{C}$ ratio is an
32 appropriate proxy to use to estimate the intrinsic state of degradation. Therefore, the $\delta^{13}\text{C}$
33 indicate a significant lower organic matter degradation for the thermokarst samples, implying

1 a better quality than that found in Yedoma samples. The high CPI values of the thermokarst
2 and the Yedoma organic matter (around 9 and higher) indicate fresh and less degraded
3 terrigenous organic matter (Brassell et al., 1978) for both deposits (Fig. 7d). The even
4 (significantly) higher CPI values of the Yedoma deposit organic matter indicate a better
5 quality for further decomposition (Fig. 7d) than in the thermokarst deposits.

6 Routh et al. (2014) states that other, more labile compounds like *n*-alcohols and *n*-fatty acids
7 are degraded to *n*-alkanes. Thus, an increase of *n*-alkanes (Fig. 3 and 4, absolute lipid
8 concentration column) is an indicator for cumulative decay. We do not see a decreasing trend,
9 which points to a constant low decomposition state. In addition, no increasing *n*-fatty acid CPI
10 with depth (as was shown in an arctic peat by Andersson and Meyers (2012)) was obvious.
11 (Andersson and Meyers, 2012) interpreted this to reflect fatty acid production during
12 humification, but we do not see this humification effect in our data, either in Yedoma, or in
13 the thermokarst deposits. Moreover, as indicated by the dominance of long-chain *n*-alkane
14 and *n*-fatty-acid compounds vs. compounds of shorter chain length (Höfle et al., 2013), we
15 confirm the interpretation of good organic matter preservation in both Yedoma and
16 thermokarst deposits. At first view, the hop-17(21)-ene (Fig. 7e) concentration does not show
17 a significant preservation difference between both kinds of deposits, because the Buo-04
18 Yedoma profile contains hopene concentrations in the same range as those found in
19 thermokarst deposits. However, if we focus on the median values, the Yedoma deposits again
20 appear to be slightly more strongly degraded than the thermokarst deposits. With the
21 exception of Buo-01, the HPFA index (Fig. 7f) also suggests lower degradation and better
22 organic matter quality in the thermokarst deposit profiles (Buo-05 and Buo-03). Our HPFA
23 index, introduced based on Poynter's (1989) HPA index which was tested in the Arctic
24 environment by Routh et al. (2014), is an appropriate indicator of the relative amount of the
25 labile fatty acids that remain in a sample. The uppermost samples just below the surface at
26 Buo-04, Buo-05, and Buo-01 with lower HPFA values are clearly an exception and suggest
27 the entrainment of higher proportions of material influenced by Holocene degradation. This is
28 likely caused by the fairly recent influence of an active layer or transient layer and warmer
29 permafrost temperatures. The Oleanen ratio shows a separation of Yedoma and thermokarst
30 deposits, but this ratio is dominated by numerous 0.0 measurements in the Yedoma deposits.
31 These results might be caused not only by transformation of β -amyryn to Olean-12-ene (by
32 losing the hydroxyl group) or to Olean-13(18)-ene (by losing the double bond), but also by so

1 far unknown processes in the Yedoma deposits. Thus, because of sparse data, we interpret this
2 proxy as a better Yedoma organic matter quality for further decomposition.

3 Summing up Fig. 7, thermokarst organic matter is partly less degraded compared to the
4 organic matter sequestered in Yedoma deposits (see table S1, significance for C/N, $\delta^{13}\text{C}$, and
5 the HPFA index). The CPI points in the other direction (Fig. 7 and table S1). For hop-17(21)-
6 ene, we do not see significant differences. Nevertheless, the interquartile ranges show an
7 overlap for most proxies. We interpret this as following: Compared to unaltered Yedoma
8 deposits, degradation during thermokarst processes, but also heightened amounts of OC input
9 during climatically more favorable Holocene times, are balancing each other concerning the
10 organic matter quality for future degradation. Nevertheless, as there is more carbon stored in
11 the thermokarst basins (Strauss et al. 2013), thermokarst deposits imply a higher intrinsic
12 potential to contribute greenhouse gases in a warmer future. This is supported by the acetate
13 data indicating a higher mean content for the thermokarst deposits. Acetate is an excellent
14 substrate for microbial turnover e.g. acetoclastic methanogenesis (Kotsyurbenko et al.,
15 2004). The PCA confirms the picture of little difference between the organic matter
16 preservation of the Yedoma and the thermokarst samples. Especially Fig. 6a, supported by
17 Fig. 2, reveals that Yedoma and thermokarst are composed of similar sediments. The Buo-05
18 thermokarst profile is very similar to both Yedoma profiles. The PCA of the degradation
19 proxies (Fig. 6b) also shows no clusters, but exhibits slightly better separation between both
20 kinds of deposits. Fig. 6b reveals that the C/N ratio, the $\delta^{13}\text{C}$ ratio, and the CPI are correlated.
21 This is also separately illustrated in Fig. 5a and c. Thus, these proxies seem to confirm each
22 other. The PCA of the *n*-alkane chain length points to a potential dominance of longer chain
23 alkanes in Yedoma and shorter chain alkanes in thermokarst, indicating better quality for
24 further decomposition of Yedoma samples (Höfle et al., 2013). Exceptions are the Buo-05-A-
25 01 and Buo-03-A-03 thermokarst samples which point in the same direction as the *n*-C₃₅
26 concentration.

27 The abovementioned overlap of the interquartile range (Fig. 7) and especially the PCA of the
28 biomarkers (Fig. 6b and c) show that the organic matter degradation/decomposition
29 vulnerability is heterogeneous and depends on different decomposition trajectories and
30 differing former decomposition/incorporation histories. This is likely shown in both Yedoma
31 and thermokarst deposits, covering the whole range of degradation proxy values (Fig 7b, c, e).
32 To elucidate this was one of the benefits of the applied multiproxy approach. With the

1 addition of biomarker data, it is possible to show that the permafrost organic matter
2 degradation is not a linear function of age or sediment facies, but likely a combination of
3 (interrupted) degradation cycles and a cascade of degradation steps. In particular, the
4 reasonably good organic matter preservation of thermokarst deposits reveals that the sediment
5 degradation processes do not necessarily degrade the organic matter. Potentially, the loss of
6 labile OC during thermokarst processes was compensated for by high rates of Holocene OC
7 accumulation in e.g. lake sediments. Nutrient release from thawing permafrost could have
8 stimulated lake productivity, whereas decomposition was slow because of low lake
9 temperatures, resulting in cold anoxic lake environments (Boike et al., 2013; Walter Anthony
10 et al., 2014). When the lake drained, permafrost formation rapidly recovered the sediments
11 (Jones et al., 2011) including any possibly newly-accumulated OC.

12 **4.3 Fate of organic matter**

13 The permafrost OC resilience or vulnerability is a topic of recent research (Schuur and
14 Abbott, 2011; Knoblauch et al., 2013; Hodgkins et al., 2014; Li et al., 2014; Mu et al., 2014).
15 Any warming permafrost is potentially vulnerable to thawing. The remaining important
16 question is this: What is the fate of the organic matter exposed to degradation after permafrost
17 has thawed? The lipid biomarker data discussed (CPI etc.) indicates that the organic matter in
18 the sediments was, after initial degradation processes, relatively quickly protected against
19 microbial alteration by freezing. This is confirmed by an absent degradation - depth trend
20 which reveals good organic matter quality independent of age. Thus, the very old frozen
21 organic matter is also vulnerable to degradation after thawing. This interpretation fits results
22 from studies of permafrost-affected Arctic peats (Hugelius et al., 2012; Routh et al., 2014).
23 Walter Anthony et al. (2014) found a net accumulation in thermokarst basins since the last
24 deglaciation, but predict a change to a large carbon source when permafrost thaws and the OC
25 will be available for oxidation. Due to ongoing climate warming in the Arctic, Grosse et al.
26 (2011b) suppose an increasing occurrence and magnitude of disturbance processes, especially
27 fire and thermokarst, which will accelerate permafrost degradation. Because our
28 sedimentological and biomarker proxies show a low degradation state, especially for the
29 paleocryosol sequences, we expect a significant vulnerability to microbial degradation after
30 thawing. As evidence that the OC is vulnerable when thawed, Gaglioti et al. (2014) found that
31 ~10 times more ancient OC found in permafrost was made available for degradation during
32 warm times of the Holocene (Holocene Thermal Maximum (11.7-9.0 ka) and Bølling-Allerød

1 periods) than is available today. By increased disturbances like deep surface subsidence
2 caused by thawing and the draining of excess water from melting ice in a warmer climate, the
3 Yedoma and, to a lesser degree because of lower excess ice content, the thermokarst organic
4 matter could become deeply bioavailable. The wedge-ice volume is estimated at up to ~60
5 vol% for Yedoma and up to ~10 vol% for thermokarst deposits (Ulrich et al., 2014). When
6 added to segregated ice, ~80 vol% and ~65 vol% mean sedimentary ice volume exists in
7 Yedoma and thermokarst, respectively (Strauss et al., 2013). When it becomes available and
8 is exported as dissolved OC to e.g. river systems, Vonk et al. (2013) and Mann et al. (2014)
9 found that dissolved OC (<0.45 μm) in ancient Yedoma is exceptionally biolabile. But if it is
10 not dissolved, the suspended (>0.45 μm) eroded ancient organic matter could be protected
11 from extensive degradation by organo-mineral bonds, which stabilize the organic matter
12 (Höfle et al., 2013) and, in an aquatic environment, promote rapid settling because they weigh
13 down the organic matter (Vonk et al., 2010).

14 From the modeling perspective, global-scale models are limited so far because they
15 implement one-dimensional vertical thaw only (Koven et al., 2011; Schneider von Deimling
16 et al., 2012; Schaphoff et al., 2013). Thus, the potentially labile Yedoma and thermokarst
17 deep OC pool described in this study is not realistically implemented in these models, because
18 the models disregard rapid phenomena like thermokarst processes. Thermokarst processes,
19 despite being local in nature, are widespread on the regional scale (Grosse et al., 2011a) and
20 may constitute the crucial process making the deep OC studied here microbiologically
21 available.

22 **5 Conclusions**

23 As being freeze-locked, the great amount of organic matter in the studied sediments is highly
24 decomposable. Generally, in all applied proxies there is no degradation - depth trend obvious,
25 revealing that permafrost acts like a freezer, preserving the organic matter after freezing.
26 Based on interpreting the mean values of the C/N ratio, isotope ratio ($\delta^{13}\text{C}$), and the HPFA
27 index, the thermokarst organic matter is less degraded and of better quality for degradation
28 after thawing compared to the organic matter sequestered in Yedoma deposits. The CPI data
29 suggest less degradation of the organic matter from both deposits with a higher value for
30 Yedoma organic matter. For the hop-17(21)-ene concentration no significant difference was
31 found. We do not see any conflict between these two determinations, because the interquartile
32 ranges overlap for most proxies. We interpret this to indicate a comparable magnitude of

1 organic matter quality in both kinds of deposits, but with a likely better thermokarst organic
2 matter quality for further degradation. For a modelling approach, this conclusion could be
3 extrapolated to the Laptev Sea Region as the studied deposits are akin to other Yedoma and
4 thermokarst deposits of the northeast Siberian Arctic (Schirrmeister et al. 2011a).

5 The fate of mobilized Yedoma deposit OC depends largely on the environmental conditions
6 that exist during the thermokarst processes and in the resulting thermokarst basin. In
7 conclusion, when the conditions are good for organic matter preservation, for example cold
8 (slightly above 0°C) or anoxic (lake) conditions, and reworked fossil organic matter can
9 rapidly refreeze to permafrost, good-quality organic matter for further decomposition can be
10 maintained and inputs likely compensate for losses due to thermokarst degradation.

11

12 **Author contribution**

13 J. Strauss, L. Schirrmeister, and S. Wetterich sampled and coordinated all sediment sampling
14 at the Buor Khaya field campaign in 2010. K. Mangelsdorf supported the biomarker analysis
15 and interpretation. J. Strauss carried out the laboratory analyses, except for one profile, which
16 was analyzed by L. Eichhorn. U. Herzsuh designed the statistical analyses. J. Strauss
17 planned and wrote the publication with input from all co-authors.

18 **Acknowledgements**

19 We acknowledge support of this research by the German Ministry of Education and Research
20 (the "System Laptev Sea" and "CarboPerm" (03G0836A) projects). We also thank the
21 Russian and German partners who were involved in the "Eastern Laptev Sea - Buor Khaya
22 Peninsula 2010" expedition. J. Strauss was supported by a grant by the Studienstiftung des
23 deutschen Volkes (German National Academic Foundation) and a European Research
24 Council Starting Grant (PETA-CARB, #338335).

25 **References**

26 Andersson, R. A., Kuhry, P., Meyers, P., Zebühr, Y., Crill, P., and Mörth, M.: Impacts of
27 paleohydrological changes on n-alkane biomarker compositions of a holocene peat sequence
28 in the eastern European Russian Arctic, *Organic Geochemistry*, 42, 1065-1075,
29 doi:10.1016/j.orggeochem.2011.06.020, 2011.

- 1 Andersson, R. A., and Meyers, P. A.: Effect of climate change on delivery and degradation of
2 lipid biomarkers in a Holocene peat sequence in the eastern European Russian Arctic, *Organic*
3 *Geochemistry*, 53, 63-72, doi:10.1016/j.orggeochem.2012.05.002, 2012.
- 4 Berg, B.: Litter decomposition and organic matter turnover in northern forest soils, *Forest*
5 *Ecology and Management*, 133, 13-22, doi:10.1016/S0378-1127(99)00294-7, 2000.
- 6 Blott, S. J., and Pye, K.: Gradistat: A grain size distribution and statistics package for the
7 analysis of unconsolidated sediments, *Earth Surface Processes and Landforms*, 26, 1237-
8 1248, doi:10.1002/esp.261, 2001.
- 9 Boike, J., Kattenstroth, B., Abramova, K., Bornemann, N., Chetverova, A., Fedorova, I.,
10 Fröb, K., Grigoriev, M., Grüber, M., Kutzbach, L., Langer, M., Minke, M., Muster, S., Piel,
11 K., Pfeiffer, E. M., Stoof, G., Westermann, S., Wischnewski, K., Wille, C., and Hubberten, H.
12 W.: Baseline characteristics of climate, permafrost and land cover from a new permafrost
13 observatory in the Lena River Delta, Siberia (1998-2011), *Biogeosciences*, 10, 2105-2128,
14 doi:10.5194/bg-10-2105-2013, 2013.
- 15 Brassell, S., Eglinton, G., Maxwell, J., and Philp, R.: Natural background of alkanes in the
16 aquatic environment. In: *Aquatic pollutants: Transformation and biological effects*, Hutzinger,
17 O., Lelyveld, I. H., and Zoetman, B. C. J. (Eds.), Pergamon Press, Oxford, 1978.
- 18 Bray, E. E., and Evans, E. D.: Distribution of n-paraffins as a clue to recognition of source
19 beds, *Geochimica et Cosmochimica Acta*, 22, 2-15, doi:10.1016/0016-7037(61)90069-2,
20 1961.
- 21 Ciais, P., Tagliabue, A., Cuntz, M., Bopp, L., Scholze, M., Hoffmann, G., Lourantou, A.,
22 Harrison, S. P., Prentice, I. C., Kelley, D. I., Koven, C., and Piao, S. L.: Large inert carbon
23 pool in the terrestrial biosphere during the last glacial maximum, *Nature Geoscience*, 5, 74-
24 79, doi:10.1038/ngeo1324, 2012.
- 25 Dlugokencky, E., and Tans, P.: Trends in atmospheric carbon dioxide:
26 <http://www.esrl.noaa.gov/gmd/ccgg/trends/global.html>, access: 23.03.2014, 2014.
- 27 Drachev, S. S., Savostin, L. A., Groshev, V. G., and Bruni, I. E.: Structure and geology of the
28 continental shelf of the Laptev Sea, eastern Russian Arctic, *Tectonophysics*, 298, 357-393,
29 doi:10.1016/S0040-1951(98)00159-0, 1998.

1 Drozdov, D. S., Rivkin, F. M., Rachold, V., Ananjeva-Malkova, G. V., Ivanova, N. V.,
2 Chehina, I. V., Koreisha, M. M., Korostelev, Y. V., and Melnikov, E. S.: Electronic atlas of
3 the Russian Arctic coastal zone, *Geo-Marine Letters*, 25, 81-88, doi:10.1007/s00367-004-
4 0189-7, 2005.

5 Folk, R. L., and Ward, W. C.: Brazos river bar: A study in the significance of grain size
6 parameters, *Journal of Sedimentary Petrology*, 27, 3-26, 1957.

7 Gaglioti, B. V., Mann, D. H., Jones, B. M., Pohlman, J. W., Kunz, M. L., and Wooller, M. J.:
8 Radiocarbon age-offsets in an Arctic lake reveal the long-term response of permafrost carbon
9 to climate change, *Journal of Geophysical Research: Biogeosciences*, 119, 1630–1651,
10 doi:10.1002/2014jg002688, 2014.

11 Glombitza, C., Mangelsdorf, K., and Horsfield, B.: Maturation related changes in the
12 distribution of ester bound fatty acids and alcohols in a coal series from the New Zealand coal
13 band covering diagenetic to catagenetic coalification levels, *Organic Geochemistry*, 40, 1063-
14 1073, doi:10.1016/j.orggeochem.2009.07.008, 2009.

15 Goslar, T., Czernik, J., and Goslar, E.: Low-energy ^{14}C AMS in Poznań radiocarbon laboratory,
16 Poland, *Nuclear Instruments and Methods in Physics Research Section B: Beam Interactions
17 with Materials and Atoms*, 223–224, 5-11, doi:10.1016/j.nimb.2004.04.005, 2004.

18 Grosse, G., Harden, J., Turetsky, M. R., McGuire, A. D., Camill, P., Tarnocai, C., Frolking,
19 S., Schuur, E. A. G., Jorgenson, T., Marchenko, S., Romanovsky, V., Wickland, K. P.,
20 French, N., Waldrop, M. P., Bourgeau-Chavez, L., and Striegl, R. G.: Vulnerability of high-
21 latitude soil organic carbon in North America to disturbance, *Journal of Geophysical
22 Research*, 116, G00K06, doi:10.1029/2010JG001507, 2011a.

23 Grosse, G., Romanovsky, V., Jorgenson, T., Anthony, K. W., Brown, J., and Overduin, P. P.:
24 Vulnerability and feedbacks of permafrost to climate change, *Eos, Transactions American
25 Geophysical Union*, 92, 73-74, doi:10.1029/2011eo090001, 2011b.

26 Grosse, G., Robinson, J. E., Bryant, R., Taylor, M. D., Harper, W., DeMasi, A., Kyker-
27 Snowman, E., Veremeeva, A., Schirrmeister, L., and Harden, J.: Distribution of late
28 Pleistocene ice-rich syngenetic permafrost of the yedoma suite in east and central Siberia,
29 Russia, U.S. Geological Survey Open File Report, 1078, U.S. Geological Survey, Reston,
30 USA, 37 pp, 2013.

1 Gubin, S. V., and Veremeeva, A. A.: Parent materials enriched in organic matter in the
2 northeast of Russia, *Eurasian Soil Science*, 43, 1238-1243, doi:10.1134/s1064229310110062,
3 2010.

4 Gundelwein, A., Muller-Lupp, T., Sommerkorn, M., Haupt, E. T. K., Pfeiffer, E., and
5 Wiechmann, H.: Carbon in tundra soils in the lake labaz region of Arctic Siberia, *European*
6 *Journal of Soil Science*, 58, pp. 1164-1174, 2007.

7 Günther, F., Overduin, P. P., Sandakov, A., Grosse, G., and Grigoriev, M. N.: Thermo-
8 erosion along the yedoma coast of the Buor Khaya peninsula, Laptev Sea, east Siberia,
9 *Proceedings of the Tenth International Conference on Permafrost, Volume 1: International*
10 *Contributions, Salekhard, Russia, 25-29 June 2012*, 137-142, 2012

11 Günther, F., Overduin, P. P., Sandakov, A. V., Grosse, G., and Grigoriev, M. N.: Short- and
12 long-term thermo-erosion of ice-rich permafrost coasts in the Laptev Sea region,
13 *Biogeosciences*, 10, 4297-4318, doi:10.5194/bg-10-4297-2013, 2013.

14 Heyer, J., Hübner, H., and Maaß, I.: Isotopenfraktionierung des Kohlenstoffs bei der
15 mikrobiellen Methanbildung, *Isotopes in Environmental and Health Studies*, 12, 202–205,
16 doi:10.1080/10256017608543912, 1976.

17 Hodgkins, S. B., Tfaily, M. M., McCalley, C. K., Logan, T. A., Crill, P. M., Saleska, S. R.,
18 Rich, V. I., and Chanton, J. P.: Changes in peat chemistry associated with permafrost thaw
19 increase greenhouse gas production, *Proceedings of the National Academy of Sciences*, 111,
20 5819-5824, doi:10.1073/pnas.1314641111, 2014.

21 Höfle, S., Rethemeyer, J., Mueller, C. W., and John, S.: Organic matter composition and
22 stabilization in a polygonal tundra soil of the Lena Delta, *Biogeosciences*, 10, 3145-3158,
23 doi:10.5194/bg-10-3145-2013, 2013.

24 Hugelius, G., Routh, J., Kuhry, P., and Crill, P.: Mapping the degree of decomposition and
25 thaw remobilization potential of soil organic matter in discontinuous permafrost terrain,
26 *Journal of Geophysical Research: Biogeosciences*, 117, G02030, doi:10.1029/2011jg001873,
27 2012.

28 Hugelius, G., Strauss, J., Zubrzycki, S., Harden, J., Schuur, E. A. G., Ping, C.-L.,
29 Schirmermeister, L., Grosse, G., Michaelson, G., Koven, C., O'Donnell, J., Elberling, B., Mishra,
30 U., Camill, P., Yu, Z., Palmtag, J., and Kuhry, P.: Estimated stocks of circumpolar permafrost

1 carbon with quantified uncertainty ranges and identified data gaps, *Biogeosciences*, 11, 6573–
2 6593, doi:10.5194/bg-11-6573-2014, 2014.

3 Jenkinson, D. S., Poulton, P. R., and Bryant, C.: The turnover of organic carbon in subsoils.
4 Part 1. Natural and bomb radiocarbon in soil profiles from the Rothamsted long-term field
5 experiments, *European Journal of Soil Science*, 59, 391-399, doi:10.1111/j.1365-
6 2389.2008.01025.x, 2008.

7 Jones, B. M., Grosse, G., Arp, C. D., Jones, M. C., Walter Anthony, K. M., and Romanovsky,
8 V. E.: Modern thermokarst lake dynamics in the continuous permafrost zone, northern
9 Seward Peninsula, Alaska, *J. Geophys. Res.*, 116, G00M03, doi:10.1029/2011JG001666,
10 2011.

11 Knoblauch, C., Beer, C., Sosnin, A., Wagner, D., and Pfeiffer, E.-M.: Predicting long-term
12 carbon mineralization and trace gas production from thawing permafrost of northeast Siberia,
13 *Glob. Change Biol.*, 19, 1160–1172, doi:10.1111/gcb.12116, 2013.

14 Kotsyurbenko, O. R., Chin, K.-J., Glagolev, M. V., Stubner, S., Simankova, M. V.,
15 Nozhevnikova, A. N., and Conrad, R.: Acetoclastic and hydrogenotrophic methane
16 production and methanogenic populations in an acidic West-Siberian peat bog, *Environmental*
17 *Microbiology*, 6, 1159-1173, doi:10.1111/j.1462-2920.2004.00634.x, 2004.

18 Koven, C. D., Ringeval, B., Friedlingstein, P., Ciais, P., Cadule, P., Khvorostyanov, D.,
19 Krinner, G., and Tarnocai, C.: Permafrost carbon-climate feedbacks accelerate global
20 warming, *Proceedings of the National Academy of Sciences*, 108, 14769-14774,
21 doi:10.1073/pnas.1103910108, 2011.

22 Kuesel, K., and Drake, H. L.: Effects of environmental parameters on the formation and
23 turnover of acetate by forest soils, *Applied and environmental microbiology*, 61, 3667-3675,
24 1995.

25 Kuhry, P., and Vitt, D. H.: Fossil carbon/nitrogen ratios as a measure of peat decomposition,
26 *Ecology*, 77, 271-275, doi:10.2307/2265676, 1996.

27 Kuhry, P., Ping, C.-L., Schuur, E. A. G., Tarnocai, C., and Zimov, S.: Report from the
28 international permafrost association: Carbon pools in permafrost regions, *Permafrost*
29 *Periglacial Process.*, 20, 229-234, doi:10.1002/ppp.648, 2009.

1 Kumada, K.: Chemistry of soil organic matter, Developments in soil science, Elsevier/Japan
2 Scientific Societies Press, Amsterdam, 1987.

3 Lee, H., Schuur, E. A. G., Inglett, K. S., Lavoie, M., and Chanton, J. P.: The rate of
4 permafrost carbon release under aerobic and anaerobic conditions and its potential effects on
5 climate, *Glob. Change Biol.*, 18, 515-527, doi:10.1111/j.1365-2486.2011.02519.x, 2012.

6 Li, J., Luo, Y., Natali, S., Schuur, E. A. G., Xia, J., Kowalczyk, E., and Wang, Y.: Modeling
7 permafrost thaw and ecosystem carbon cycle under annual and seasonal warming at an Arctic
8 tundra site in Alaska, *Journal of Geophysical Research: Biogeosciences*, 119, 2013JG002569,
9 doi:10.1002/2013jg002569, 2014.

10 Luo, Q., Yu, S., Liu, Y., Zhang, Y., Han, H., Qi, L., and Zhong, N.: Existence and
11 implications of hop-17(21)-enes in the lower cretaceous of the Saihantala Sag, Erlian Basin,
12 China, *Pet. Sci.*, 9, 154-160, doi:10.1007/s12182-012-0195-8, 2012.

13 Mangelsdorf, K., Finsel, E., Liebner, S., and Wagner, D.: Temperature adaptation of
14 microbial communities in different horizons of Siberian permafrost-affected soils from the
15 Lena Delta, *Chemie der Erde - Geochemistry*, 69, 169-182,
16 doi:10.1016/j.chemer.2009.02.001, 2009.

17 Mann, P. J., Sobczak, W. V., LaRue, M. M., Bulygina, E., Davydova, A., Vonk, J. E., Schade,
18 J., Davydov, S., Zimov, N., Holmes, R. M., and Spencer, R. G. M.: Evidence for key
19 enzymatic controls on metabolism of Arctic river organic matter, *Glob. Change Biol.*, 20,
20 1089-1100, doi:10.1111/gcb.12416, 2014.

21 Marzi, R., Torkelson, B. E., and Olson, R. K.: A revised carbon preference index, *Organic*
22 *Geochemistry*, 20, 1303-1306, doi:10.1016/0146-6380(93)90016-5, 1993.

23 McKane, R. B., Rastetter, E. B., Shaver, G. R., Nadelhoffer, K. J., Giblin, A. E., Laundre, J.
24 A., and Chapin, F. S.: Climatic effects on tundra carbon storage inferred from experimental
25 data and a model, *Ecology*, 78, 1170-1187, doi:10.1890/0012-
26 9658(1997)078[1170:ceotcs]2.0.co;2, 1997.

27 Mu, C., Zhang, T., Schuster, P. F., Schaefer, K., Wickland, K. P., Repert, D. A., Liu, L.,
28 Schaefer, T., and Cheng, G.: Carbon and geochemical properties of cryosols on the north
29 slope of Alaska, *Cold Regions Science and Technology*, 100, 59-67,
30 doi:10.1016/j.coldregions.2014.01.001, 2014.

- 1 Oksanen, J.: Multivariate analysis of ecological communities in r: Vegan tutorial, University
2 of Oulu, Oulu, 43 pp., 2013.
- 3 Ping, C. L., Bockheim, J. G., Kimble, J. M., Michaelson, G. J., and Walker, D. A.:
4 Characteristics of cryogenic soils along a latitudinal transect in Arctic Alaska, *Journal of*
5 *Geophysical Research: Atmospheres*, 103, 28917-28928, doi:10.1029/98jd02024, 1998.
- 6 Poynter, J., and Eglinton, G.: 14. Molecular composition of three sediments from hole 717c:
7 The Bengal fan, *Proceedings of the Ocean Drilling Program: Scientific results*, 116, 155-161,
8 1990.
- 9 Poynter, J.: Molecular stratigraphy: The recognition of palaeoclimatic signals in organic
10 geochemical data, PhD, School of Chemistry, University of Bristol, Bristol, 324 pp., 1989.
- 11 Radke, M., Willsch, H., and Welte, D. H.: Preparative hydrocarbon group type determination
12 by automated medium pressure liquid chromatography, *Analytical Chemistry*, 52, 406-411,
13 doi:10.1021/ac50053a009, 1980.
- 14 Romanovskii, N. N., Hubberten, H. W., Gavrillov, A. V., Tumskey, V. E., and Kholodov, A.
15 L.: Permafrost of the east Siberian Arctic shelf and coastal lowlands, *Quaternary Science*
16 *Reviews*, 23, 1359-1369, doi:10.1016/j.quascirev.2003.12.014, 2004.
- 17 Romanovsky, V. E., Smith, S. L., and Christiansen, H. H.: Permafrost thermal state in the
18 polar northern hemisphere during the international polar year 2007–2009: A synthesis,
19 *Permafrost Periglacial Process.*, 21, 106-116, doi:10.1002/ppp.689, 2010.
- 20 Routh, J., Hugelius, G., Kuhry, P., Filley, T., Tillman, P. K., Becher, M., and Crill, P.: Multi-
21 proxy study of soil organic matter dynamics in permafrost peat deposits reveal vulnerability
22 to climate change in the European Russian Arctic, *Chemical Geology*, 368, 104-117,
23 doi:10.1016/j.chemgeo.2013.12.022, 2014.
- 24 Rumpel, C., and Kögel-Knabner, I.: Deep soil organic matter - a key but poorly understood
25 component of terrestrial c cycle, *Plant Soil*, 338, 143-158, doi:10.1007/s11104-010-0391-5,
26 2011.
- 27 Schädel, C., Schuur, E. A. G., Bracho, R., Elberling, B., Knoblauch, C., Lee, H., Luo, Y. Q.,
28 Shaver, G. R., and Turetsky, M. R.: Circumpolar assessment of permafrost C quality and its
29 vulnerability over time using long-term incubation data, *Glob. Change Biol.*, 20, 641-652,
30 doi:10.1111/gcb.12417, 2014.

1 Schaphoff, S., Heyder, U., Ostberg, S., Gerten, D., Heinke, J., and Lucht, W.: Contribution of
2 permafrost soils to the global carbon budget, *Environmental Research Letters*, 8, 014026,
3 doi:10.1088/1748-9326/8/1/014026, 2013.

4 Schirrmeister, L., Grosse, G., Wetterich, S., Overduin, P. P., Strauss, J., Schuur, E. A. G., and
5 Hubberten, H.-W.: Fossil organic matter characteristics in permafrost deposits of the northeast
6 Siberian Arctic, *Journal of Geophysical Research*, 116, G00M02, doi:10.1029/2011jg001647,
7 2011a.

8 Schirrmeister, L., Kunitsky, V., Grosse, G., Wetterich, S., Meyer, H., Schwamborn, G.,
9 Babi, O., Derevyagin, A., and Siegert, C.: Sedimentary characteristics and origin of the late
10 pleistocene ice complex on north-east Siberian Arctic coastal lowlands and islands - a review,
11 *Quaternary International*, 241, 3-25, doi:10.1016/j.quaint.2010.04.004, 2011b.

12 Schirrmeister, L., Froese, D. G., Tumskey, V., Grosse, G., and Wetterich, S.: Yedoma: late
13 Pleistocene ice-rich syngenetic permafrost of Beringia, in: *Encyclopedia of quaternary
14 sciences*, 2 ed., edited by: Elias, S. A., Quaternary glaciation | cold regions landforms,
15 Elsevier, Amsterdam, 2013.

16 Schneider von Deimling, T., Meinshausen, M., Levermann, A., Huber, V., Frieler, K.,
17 Lawrence, D. M., and Brovkin, V.: Estimating the near-surface permafrost-carbon feedback
18 on global warming, *Biogeosciences*, 9, 649-665, cc, 2012.

19 Schulte, S., Mangelsdorf, K., and Rullkötter, J.: Organic matter preservation on the Pakistan
20 continental margin as revealed by biomarker geochemistry, *Organic Geochemistry*, 31, 1005-
21 1022, doi:10.1016/S0146-6380(00)00108-X, 2000.

22 Schuur, E. A. G., Vogel, J. G., Crummer, K. G., Lee, H., Sickman, J. O., and Osterkamp, T.
23 E.: The effect of permafrost thaw on old carbon release and net carbon exchange from tundra,
24 *Nature*, 459, 556-559, doi:10.1038/nature08031, 2009.

25 Schuur, E. A. G., and Abbott, B.: High risk of permafrost thaw, *Nature*, 480, 32-33,
26 doi:10.1038/480032a, 2011.

27 Shirokova, L. S., Pokrovsky, O. S., Kirpotin, S. N., Desmukh, C., Pokrovsky, B. G., Audry,
28 S., and Viers, J.: Biogeochemistry of organic carbon, CO₂, CH₄, and trace elements in
29 thermokarst water bodies in discontinuous permafrost zones of Western Siberia,
30 *Biogeochemistry*, 113, 573-593, doi:10.1007/s10533-012-9790-4, 2013.

- 1 Smith, M. R., and Mah, R. A.: Acetate as sole carbon and energy source for growth of
2 methanosarcina strain 227, *Applied and environmental microbiology*, 39, 993-999, 1980.
- 3 Sollins, P., Spycher, G., and Glassman, C. A.: Net nitrogen mineralization from light- and
4 heavy-fraction forest soil organic matter, *Soil Biology and Biochemistry*, 16, 31-37,
5 doi:10.1016/0038-0717(84)90122-6, 1984.
- 6 Stevenson, F. J.: *Humus chemistry: Genesis, composition, reactions*, John Wiley & Sons,
7 New York, 1994.
- 8 Strauss, J., and Schirrmeister, L.: Permafrost sequences of buor khaya peninsula, in: *Reports*
9 *on polar and marine research - Russian-German cooperation system Laptev Sea: The*
10 *expedition eastern Laptev Sea-Buor Khaya Peninsula 2010*, edited by: Wetterich, S.,
11 Overduin, P. P., and Grigoriev, M., Alfred Wegener Institute for Polar and Marine Research,
12 Bremerhaven, Germany, 35-50, 2011.
- 13 Strauss, J., Schirrmeister, L., Wetterich, S., Borchers, A., and Davydov, S. P.: Grain-size
14 properties and organic-carbon stock of yedoma ice complex permafrost from the Kolyma
15 lowland, northeastern Siberia, *Global Biogeochemical Cycles*, 26, GB3003,
16 doi:10.1029/2011GB004104, 2012.
- 17 Strauss, J., Schirrmeister, L., Grosse, G., Wetterich, S., Ulrich, M., Herzsuh, U., and
18 Hubberten, H.-W.: The deep permafrost carbon pool of the yedoma region in Siberia and
19 Alaska, *Geophys. Res. Lett.*, 40, 6165–6170, doi:10.1002/2013GL058088, 2013.
- 20 Stuiver, M., Reimer, P., and Reimer, R.: *Calib 6.0*, in, ¹⁴C CHRONO Centre, Queens
21 University Belfast, Belfast, 2010.
- 22 Tieszen, L.: Photosynthesis and respiration in Arctic tundra grasses: Field light intensity and
23 temperature responses, *Arctic and Alpine Research*, 5, 239-251, 1973.
- 24 Ulrich, M., Grosse, G., Strauss, J., and Schirrmeister, L.: Quantifying wedge-ice volumes in
25 yedoma and thermokarst basin deposits, *Permafrost Periglacial Process.*, 25, 151–161,
26 doi:10.1002/ppp.1810, 2014.
- 27 van Huissteden, J., and Dolman, A. J.: Soil carbon in the Arctic and the permafrost carbon
28 feedback, *Current Opinion in Environmental Sustainability*, 4, 545-551,
29 doi:10.1016/j.cosust.2012.09.008, 2012.

1 Vieth, A., Mangelsdorf, K., Sykes, R., and Horsfield, B.: Water extraction of coals – potential
2 for estimating low molecular weight organic acids as carbon feedstock for the deep terrestrial
3 biosphere, *Organic Geochemistry*, 39, 985-991, doi:10.1016/j.orggeochem.2008.02.012,
4 2008.

5 Vonk, J. E., Sánchez-García, L., Semiletov, I., Dudarev, O., Eglinton, T., Andersson, A., and
6 Gustafsson, Ö.: Molecular and radiocarbon constraints on sources and degradation of
7 terrestrial organic carbon along the Kolyma paleoriver transect, east Siberian Sea,
8 *Biogeosciences*, 7, 3153-3166, doi:10.5194/bg-7-3153-2010, 2010.

9 Vonk, J. E., Mann, P. J., Davydov, S., Davydova, A., Spencer, R. G. M., Schade, J., Sobczak,
10 W. V., Zimov, N., Zimov, S., Bulygina, E., Eglinton, T. I., and Holmes, R. M.: High
11 biolability of ancient permafrost carbon upon thaw, *Geophys. Res. Lett.*, 40, 2689-2693,
12 doi:10.1002/grl.50348, 2013.

13 Waldrop, M. P., Wickland, K. P., White Iii, R., Berhe, A. A., Harden, J. W., and
14 Romanovsky, V. E.: Molecular investigations into a globally important carbon pool:
15 Permafrost-protected carbon in Alaskan soils, *Glob. Change Biol.*, 16, 2543-2554,
16 doi:10.1111/j.1365-2486.2009.02141.x, 2010.

17 Walter Anthony, K. M., Zimov, S. A., Grosse, G., Jones, M. C., Anthony, P. M., Chapin III,
18 F. S., Finlay, J. C., Mack, M. C., Davydov, S., Frenzel, P., and Frolking, S.: A shift of
19 thermokarst lakes from carbon sources to sinks during the Holocene epoch, *Nature*, 511, 452–
20 456, doi:10.1038/nature13560, 2014.

21 Walter, K. M., Edwards, M. E., Grosse, G., Zimov, S. A., and Chapin, F. S.: Thermokarst
22 lakes as a source of atmospheric CH₄ during the last deglaciation, *Science*, 318, 633-636,
23 doi:10.1126/science.1142924, 2007a.

24 Walter, K. M., Smith, L. C., and Chapin, S. F.: Methane bubbling from northern lakes:
25 Present and future contributions to the global methane budget, *Philosophical Transactions of*
26 *the Royal Society A: Mathematical, Physical and Engineering Sciences*, 365, 1657-1676,
27 doi:10.1098/rsta.2007.2036, 2007b.

28 Weintraub, M. N., and Schimel, J. P.: Nitrogen cycling and the spread of shrubs control
29 changes in the carbon balance of Arctic tundra ecosystems, *BioScience*, 55, 408-415,
30 doi:10.1641/0006-3568(2005)055[0408:ncatso]2.0.co;2, 2005.

1 Zanina, O. G., Gubin, S. V., Kuzmina, S. A., Maximovich, S. V., and Lopatina, D. A.: Late-
2 Pleistocene (MIS 3-2) palaeoenvironments as recorded by sediments, palaeosols, and ground-
3 squirrel nests at Duvanny Yar, Kolyma Lowland, northeast Siberia, *Quaternary Science*
4 *Reviews*, 30, 2107–2123, doi:10.1016/j.quascirev.2011.01.021, 2011.

5

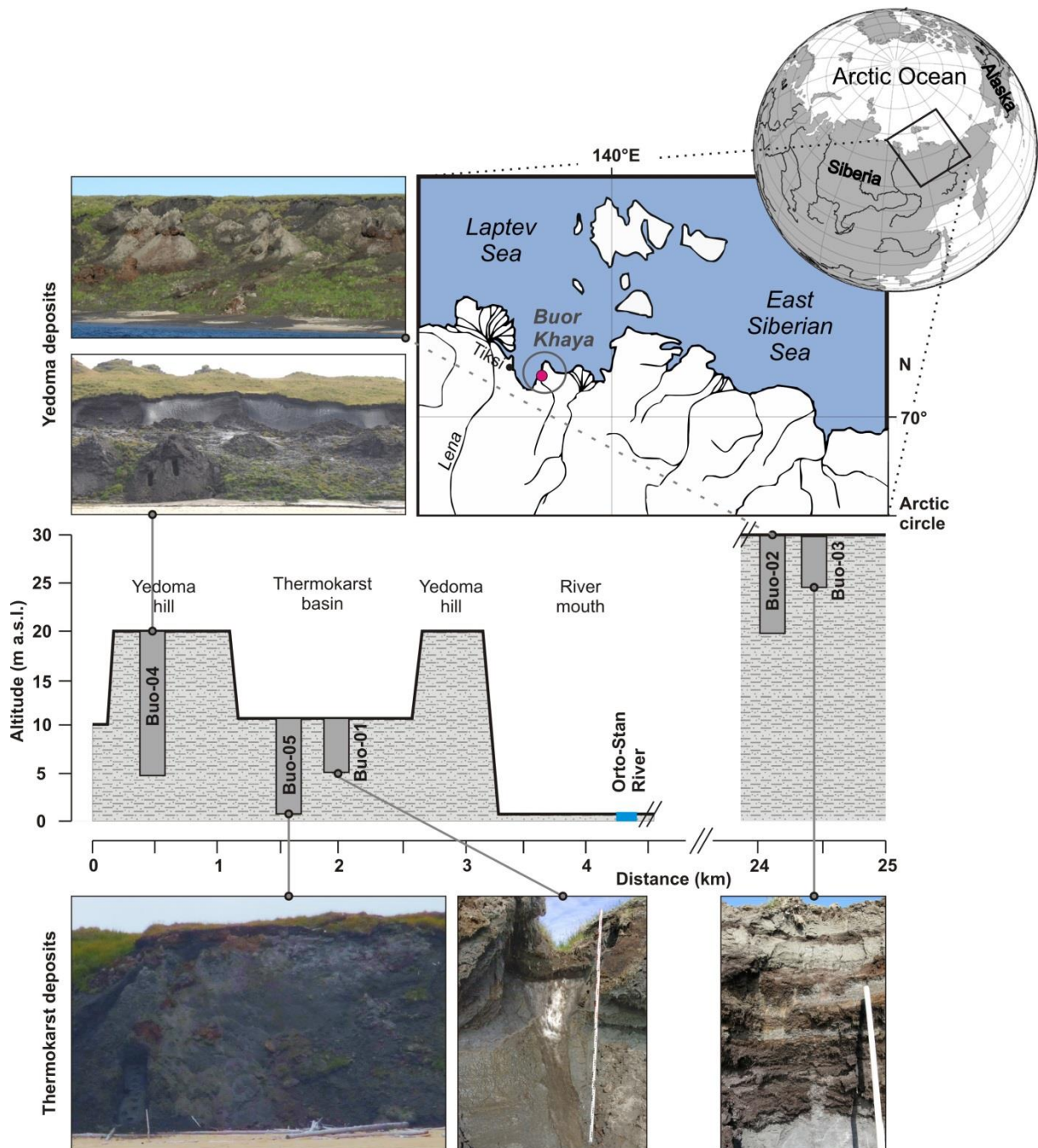
1 Table 1: Radiocarbon AMS dating on plant macro remains. Calibrations were done by using
 2 Calib 6.0 software and the IntCal09 calibration curve (Stuiver et al., 2010). Depth is given in
 3 meter below surface level (m b.s.l.) and height in meter above sea level (m a.s.l.). Age is
 4 given as year before present (a BP). Poz: Poznań Radiocarbon Laboratory, Poland.

Lab. no.	Sample name	Depth [m b.s.l.]	Height [m a.s.l.]	Radiocarbon ages [a BP]	±	Calibrated ages 2σ 95.4% [a BP]	±
Poz-42080	Buo-03-A-03	1.3	28.7	4760	40	5519	70
Poz-42072	Buo-01-A-02	0.7	8.7	3665	35	3990	100
Poz-42073	Buo-01-A-04	1.8	7.6	8140	50	9075	78
Poz-42086	Buo-05-A-04	0.8	8.7	5990	40	6837	103
Poz-42087	Buo-05-B-10	3.4	6.1	8000	80	8817	215
Poz-42088	Buo-05-B-19	6.1	3.4	7940	50	8811	122
Poz-42090	Buo-05-C-23	7.3	2.2	5280	35	6059	74
Poz-42091	Buo-05-C-29	9.2	0.3	6710	90	7566	138
Poz-42074	Buo-02-A-03	0.7	29.3	30,100	300	34613	596
Poz-42075	Buo-02-B-09	3.5	26.5	34,650	550	39813	1242
Poz-42076	Buo-02-B-12	5	25	41,500	1500	45312	2649
Poz-42077	Buo-02-D-20	5.5	24.5	45,000	2000	47614	2386
Poz-42078	Buo-02-D-23	7	23	43,000	1500	46,830	2678
Poz-42081	Buo-04-A-02	1.5	17.1	49,000	3000		
Poz-42082	Buo-04-A-08	5	13.6	>48,000			
Poz-42083	Buo-04-B-10	8.5	9.1	>55,000			
Poz-42084	Buo-04-C-16	10.5	8	>49,000			
Poz-42085	Buo-04-C-20	11.7	6.8	>55,000			

thermocarst deposits

Yedoma deposits

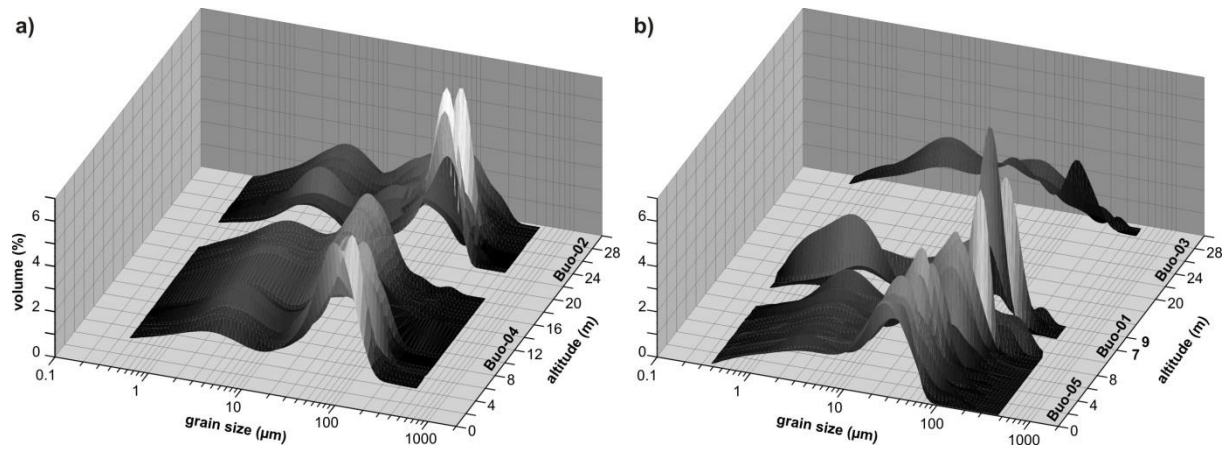
5



1

2 Figure 1. Location of the Buor Khaya Peninsula and the study area. The square black box in
 3 the globe inset indicates the area shown in the map below. The profile diagram and the
 4 photographs below it show the profiles and their positions relative to each other. Modified
 5 after Strauss and Schirmer (2011), pictures taken by J. Strauss.

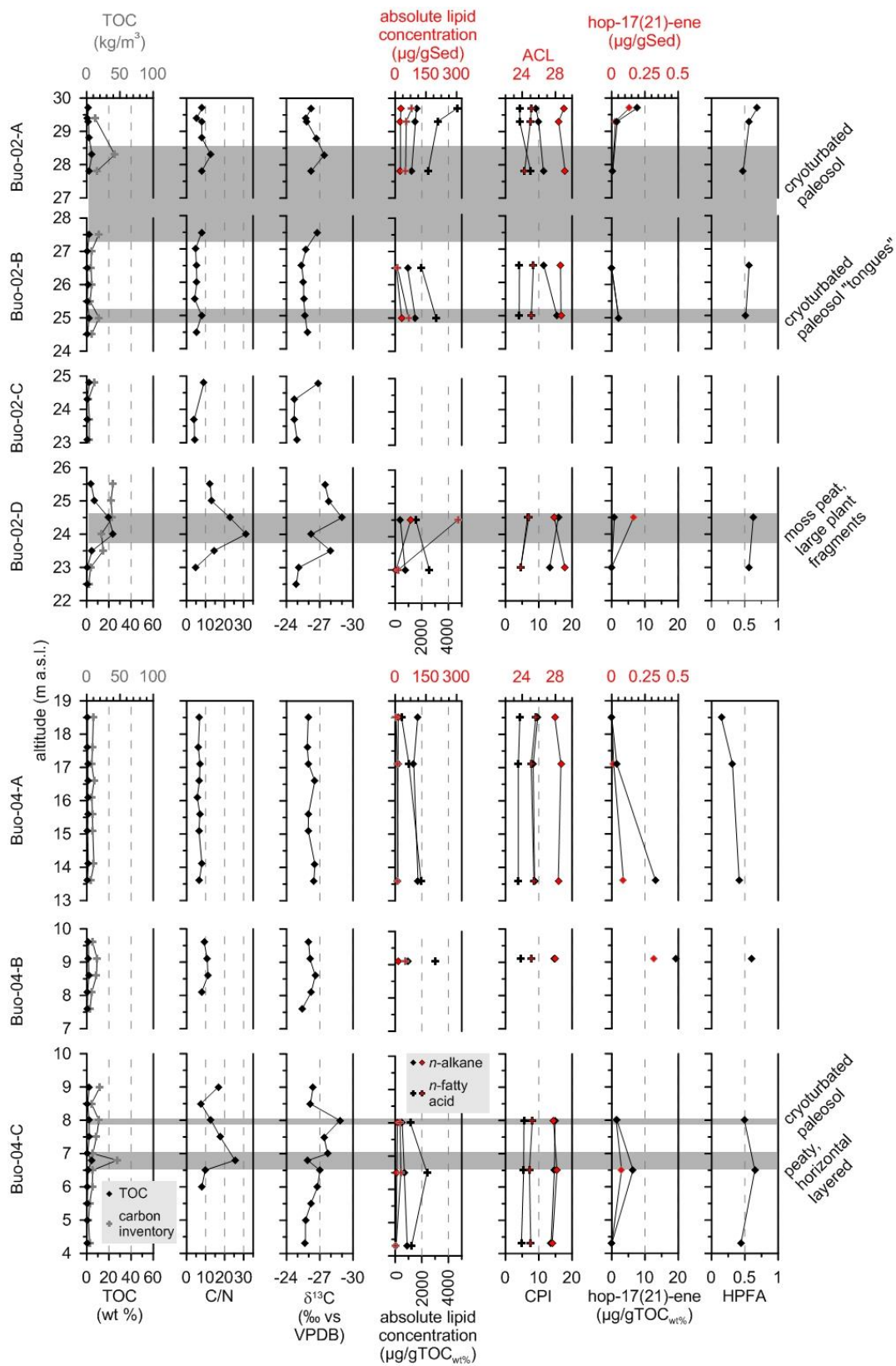
6



1

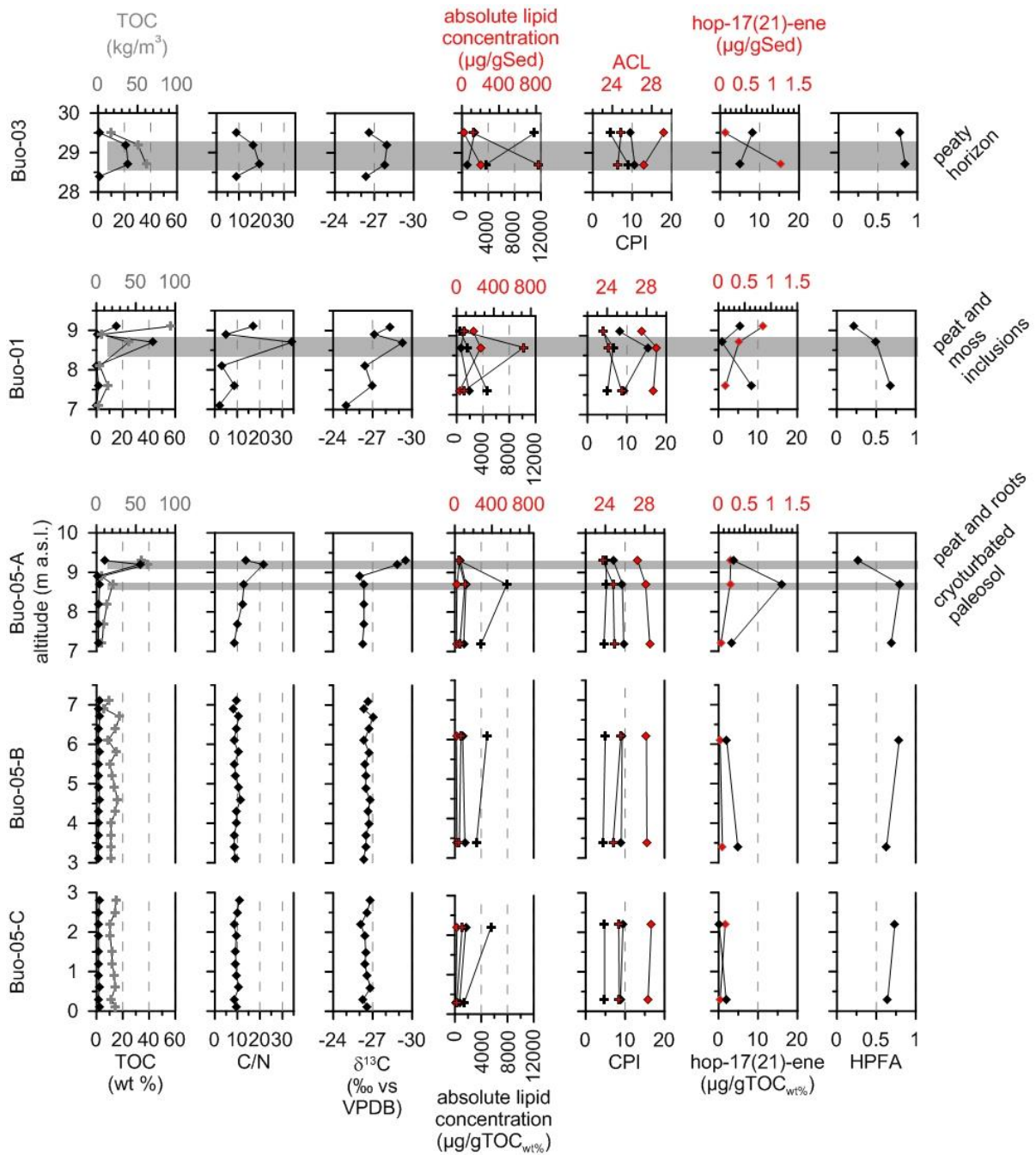
2 Figure 2. Three-dimensional grain-size distributions of a) Yedoma and b) thermokarst
 3 profiles. To avoid an overlap of Buo-05 and Buo-01 in b), the altitude axis was adapted and
 4 does not ascend consistently. A two-dimensional grain-size plot is shown in Fig. S1.

5



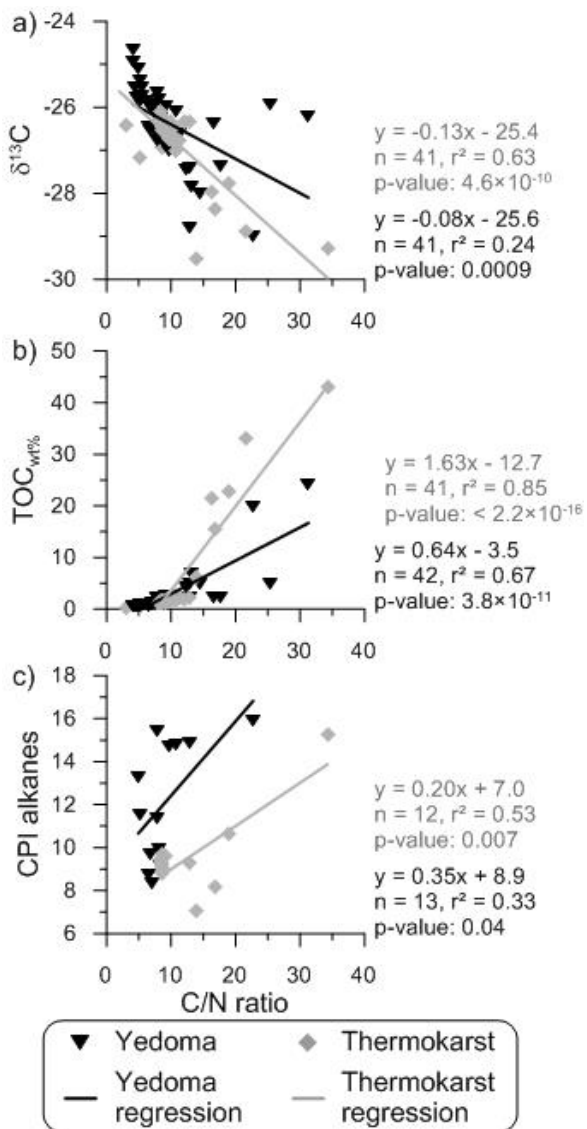
1
 2 Figure 3. Summary of sedimentological, biogeochemical, and biomarker parameters for the
 3 Buo-04 and Buo-02 Yedoma profiles. All diagrams are drawn in such a way as to show more
 4 degraded samples on the left and less degraded samples on the right side. Thus, the axis of

1 $\delta^{13}\text{C}$ values is descending. In the text, the paleocryosol parts are reported with altitude
 2 measurements from the lowest to the highest sample of each paleocryosol. The grey shaded
 3 areas are for visualization, not for exact height estimations of the paleocryosols.



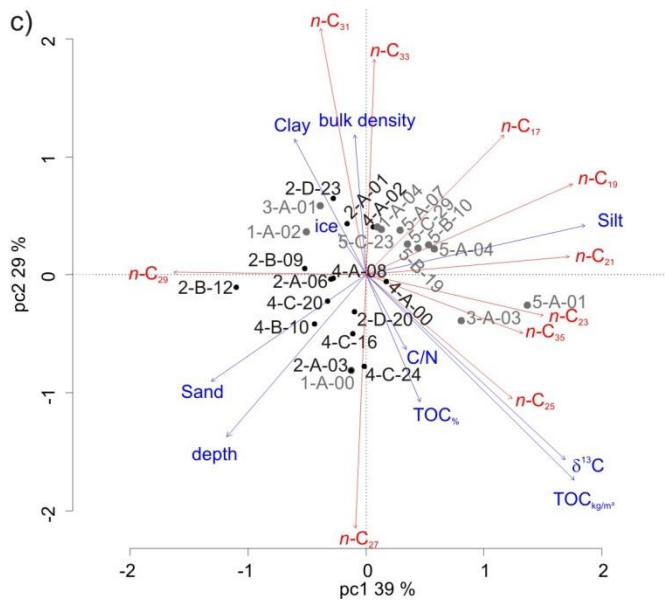
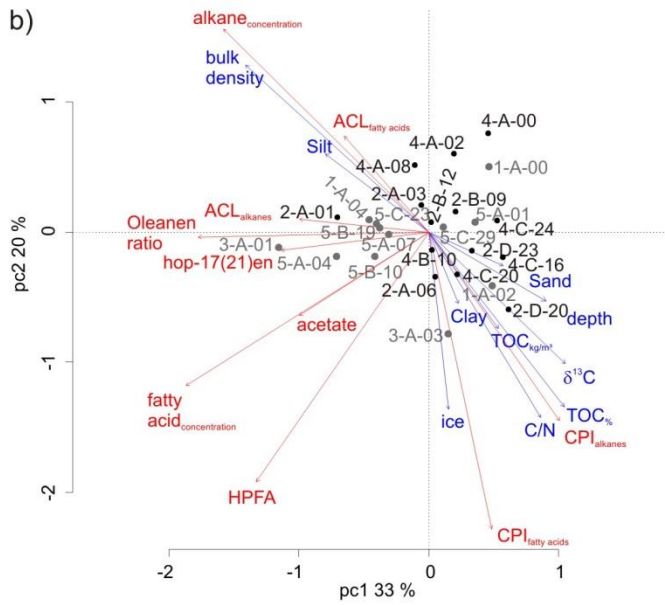
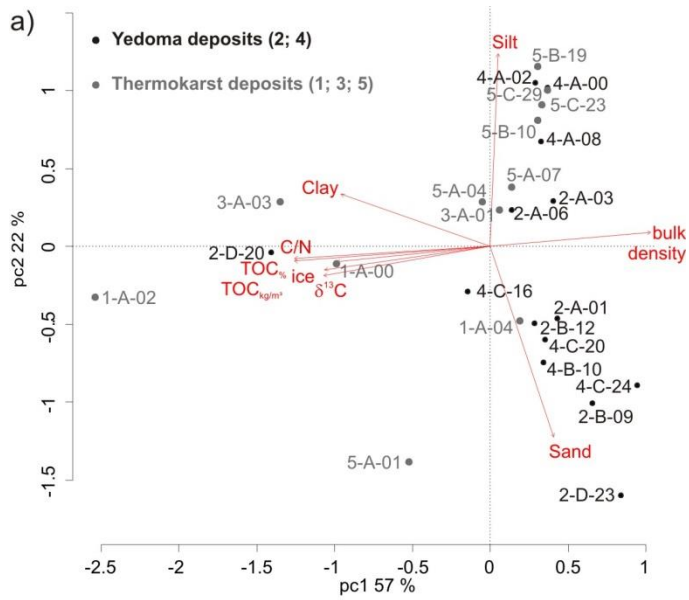
4
 5 Figure 4. Summary of sedimentological, biogeochemical, and biomarker parameters for the
 6 Buo-05, Buo-01, and Buo-03 thermokarst profiles. The *n*-alkane and *n*-fatty acid symbols are
 7 explained in Fig. 3. All diagrams are drawn in such a way as to show more degraded samples
 8 on the left and less degraded samples on the right side (descending axis of $\delta^{13}\text{C}$ values). In the
 9 text, the paleocryosol parts are reported with altitude measurements from the lowest to the

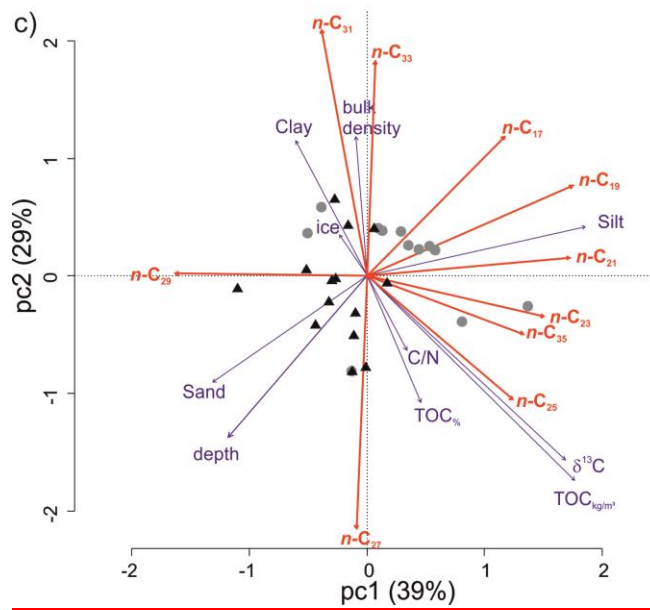
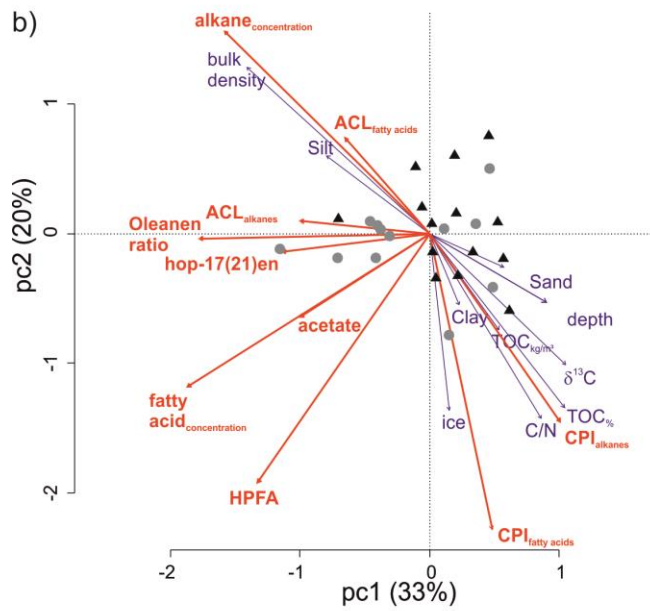
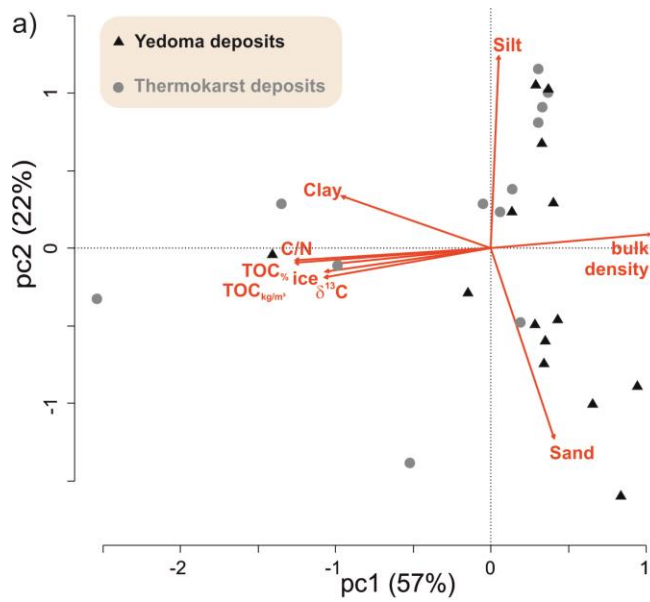
1 highest sample of each paleocryosol. The grey shaded areas are for visualization, not for exact
 2 height estimations of the paleocryosols.
 3



4
 5 Figure 5. Scatter plots of selected degradation markers. The x-axis shows the C/N ratio
 6 always. Yedomas deposits are shown as black triangles, thermokarst deposits as grey
 7 diamonds. Regression equations, the r^2 , sample number (n) and the p-value are inserted as
 8 texts.

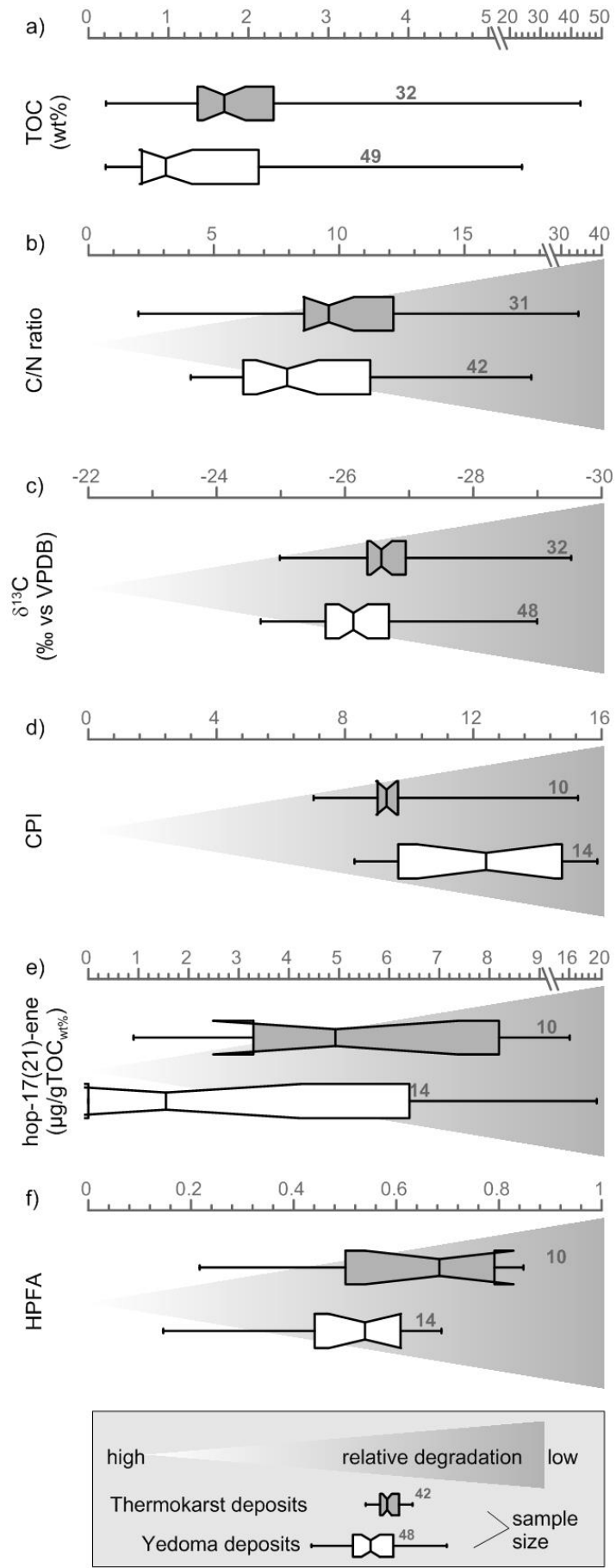
9





1 Figure 6. Ordination plots of the principal component analyses (PCA). In diagram a) the
2 sedimentological parameters are plotted. In b) a PCA of biomarker proxies is shown.
3 Supplementary variables (in blue: TOC_{wt%}, C/N, $\delta^{13}\text{C}$, grain size, BD, ice content) were added
4 without including them in the PCA calculation. In diagram c) the PCA of the major odd *n*-
5 alkanes is visualized using the same supplementary variables as in b).

6



1 Figure 7. Conceptual scheme of the organic matter degradation state, estimated using the
2 different applied proxies with boxplots. The merged profiles of Yedoma deposit boxplots
3 (white boxes) are shown below the thermokarst deposits (grey boxes). The whiskers illustrate
4 the data range, and the box ends indicate the 25th and the 75th quartile (interquartile range).
5 The vertical lines inside each box show the median (=50th quartile) including the 95%
6 confidence intervals, illustrated as notches. All diagrams are drawn in such a way as to show
7 more degraded samples on the left and less degraded samples on the right side. Thus, the axis
8 of $\delta^{13}\text{C}$ values is descending.